Journal of
Materials Chemistry C

Accepted Manuscript

This article can be cited before page numbers have been issued, to do this please use: D. Zhou, L. Pang, D. Wang and I. M. Reaney, *J. Mater. Chem. C*, 2018, DOI: 10.1039/C8TC02260G.

ROYAL SOCIETY OF CHEMISTRY

rsc.li/materials-c

View Article Online
DOI: 10.1039/C8TC02260G

$BiVO_4$ based high k microwave dielectric materials: a review

Di Zhou[*‡a,b], Li-Xia Pang[‡a,c], Da-Wei Wang[a], & Ian M. Reaney[*a]

[a]Department of Materials Science and Engineering, University of Sheffield, S1 3JD, UK

[b]Electronic Materials Research Laboratory, Key Laboratory of the Ministry of Education & International Center for Dielectric Research, School of Electronic and Information Engineering, Xi'an Jiaotong University, Xi'an 710049, China

[c]Micro-optoelectronic Systems Laboratories, Xi'an Technological University, Xi'an 710032, Shaanxi, China

[*]Corresponding author E-mail address: zhoudi1220@gmail.com (Di Zhou) & i.m.reaney@sheffield.ac.uk (Ian M. Reaney)
[‡]These authors contributed equally to this work.

View Article Online
DOI: 10.1039/C8TC02260G

Abstract

$BiVO_4$ material has attracted much attention in recent years due to its active photocatalytic properties under visible light, bright yellow color as a nontoxic pigment, and its high relative permittivity (ε_r) and *Qf* (quality factor, Q × resonant frequency, *f*) as a potential microwave dielectric ceramic. In this review, we introduce the origin, synthesis, crystal structure and phase transitions of the four polymorphic phases of $BiVO_4$: orthorhombic (pucherite), zircon (dreyerite), scheelite monoclinic (clinobisvanite) and scheelite tetragonal. We then precis recent studies on doped $BiVO_4$ ceramics in terms of A site, B site and A/B site complex substitutions. Low sintering temperature (< 800 ^oC) and high ε_r values could be obtained in some solid solution ceramics and near zero temperature coefficient of resonant frequency (TCF/τ_f) values could be achieved in layered or granulated particles composite ceramics. Besides, a series of temperature stable high ε_r microwave dielectric ceramics can also be obtained in many co-fired composite ceramics, such as $BiVO_4$-TiO_2, $BiVO_4$-TiO_2-$Bi_2Ti_4O_{11}$. The high ε_r, high Qf value, low sintering temperature and chemical compatibility with some base metals, suggest that $BiVO_4$-based materials are strong candidates for both LTCC and other microwave devices applications in current 4G and future 5G technologies.

View Article Online
DOI: 10.1039/C8TC02260G

1. Introduction

The natural mineral $BiVO_4$ crystallizes in an orthorhombic structure (pucherite) with a density 6.63 g/cm^3.[1-3] The first attempt to synthesize $BiVO_4$ using a precipitation method from Na_3VO_4 and $Bi(NO_3)_3$ led to formation of a zircon-type tetragonal $BiVO_4$ with cell parameter a = 7.290 Å, c = 6.444 Å and a density 6.25 g/cm^3.[4] The zircon-structured $BiVO_4$ transformed irreversibly to monoclinic scheelite structure (fergusonite) when heated above 400 ^{o}C. Monoclinic $BiVO_4$ with a density ~ 6.98 g/cm^3 was first synthesized by Roth and Waring in 1963 using a solid state reaction between Bi_2O_3 and V_2O_5 at > 700 ^{o}C. It melts congruently at about 940 ^{o}C.[5] Roth and Waring also found that pucherite $BiVO_4$ transformed to monoclinic when heated up to 500 ^{o}C. Considering the difference in the densities of the three polymorphs, Roth and Waring hypothesized that pucherite $BiVO_4$ might in reality be an intermediate pressure mineral formed within the earth's crust and hence could not be synthesized in the laboratory at ambient pressure.

In 1974, Dudnik et al.[6] first reported that monoclinic $BiVO_4$ single crystal underwent a ferroelastic phase transition at about 230 ^{o}C. At the same time, Bierlein and Sleight,[7] using in-situ optical and XRD techniques, found that the room temperature monoclinic $BiVO_4$ phase had a body-centered monoclinic structure with space group I2/a which transformed to an ideal scheelite structure with space group $I4_1/a$ at 255 ± 2 ^{o}C. Bierlein and Sleight claimed that the monoclinic to scheelite transition was displacive and therefore could not be suppressed by quenching. It was noted that the ferroelastic transition occurred either as a function of temperature or external pressure and was considered second order. Subsequent studies of phase transition in $BiVO_4$[8,9] using *in-situ* Raman spectroscopy,[10,11] transmission electron

View Article Online
DOI: 10.1039/C8TC02260G

microscopy,[12] *in-situ* birefringence,[13] and Brillouin spectroscopy[14] provided a consistent set of descriptive parameters for the transition, in which the lone-electron pair on the Bi^{3+} ion was thought to play a prominent role. Although there has been no direct application based on its ferroelasticity, $BiVO_4$ has been widely studied and used as a photocatalyst, for pigments and as a dielectric.[15-17]

Monoclinic $BiVO_4$ has a band gap ~ 2.4 eV and was first found to be a photocatalyst for solar oxidation by Kudo et al. in 1998[15] as it exhibits strong photocatalytic activities for O_2 evolution from aqueous silver nitrate solutions under visible light irradiation. Subsequently, $BiVO_4$ attracted much attention for suspension-type photocatalysts for water oxidation, photo-degradation of organic compounds,[18-21] and electrodes for use as photoanodes for photo-electrochemical cells. For this application, efforts were made to modify the powder morphology, construction of composite structures, doping, and pairing with oxygen evolution catalysts to further improve the photocatalytic activity of $BiVO_4$ powders.

$BiVO_4$ is also widely used as a yellow ceramic to which human eyes are quite sensitive. They replaced, early commercial yellow pigments based on lead and cadmium oxides which were hazardous to the environment. After American registered $BiVO_4$ as color index (C. I.) -184, many companies produced a series of $BiVO_4$ based yellow pigments[16,17,22-24] doped with Mo or W. $BiVO_4$ pigments are usually produced through a two-stage process in which $BiVO_4$ precipitates are synthesized by a soft chemical method and then calcined at higher temperature.

Microwave dielectric ceramics have been widely used in dielectric resonator, filter and substrates applications[25-27] for which high permittivity (ε_r) is often required to reduce device volume. In 2000, Valant and Suvorov[28] first reported the microwave dielectric properties of $BiVO_4$ ceramic with ε_r ~ 68, quality factor (reciprocal of

View Article Online
DOI: 10.1039/C8TC02260G

dielectric loss × frequency, *Qf*) ~ 6,500 GHz, and temperature coefficient of resonant frequency (TCF) ~ − 260 ppm/^{o}C, measured at a frequency of 5 GHz. However, they found that $BiVO_4$ reacted with silver at its sintering temperature to form $Bi_3AgV_2O_{10}$, prohibiting its use in low temperature co-fired ceramic (LTCC) applications. Subsequently, the microwave dielectric properties with of $BiVO_4$, *Qf* ~ 8,000 GHz, ε_r ~ 68, and TCF ~ − 243 ppm/°C were confirmed by Wee et al.[29] and it was used to lower the densification temperature of $ZnNb_2O_6$ ceramic from 1200 ^{o}C to about 925°C. However, in general, a large –ve *TCF* along with its poor compatibility with Ag internal electrodes limits the application of $BiVO_4$ in LTCC technology despite the attraction of an intrinsically low sintering temperature (820 ^{o}C).[30,31]. In 2010, $(Li_{0.5}Bi_{0.5})MoO_4$ was reported to form a full solid solution with $BiVO_4$[32] accompanied by lowering of the sintering temperature to < 660 ^{o}C. Some compositions within the solid solution $(Li_{0.5x}Bi_{1-0.5x})(Mo_xV_{1-x})O_4$ densified well and were chemically compatible with both aluminum and copper and had a less -*ve TCF* than $BiVO_4$. This result suggested that $BiVO_4$ could act as a base for the development of low sintering temperature MW dielectrics. Besides, the mobile communication technology has been driven by the 5G instead of the current 3G / 4G. In the future 5G technology with wide bandwidth, small time delay and fast transmission speed will be required to meet the demands of wirelessly connected devices in the 'Internet of Things' (IoT). 5G technology will eventually utilize high frequencies (> 24 GHz) in the so-called mm wave regime (ε_r < 10) but will initially use lower frequencies (e.g. 3 to 6 GHz) which require higher ε_r, typically from 20 to 60 to decrease device volume. The large ε_r of $BiVO_4$ based materials suggests they might be better suited to wireless communication devices rather than as resonators for which lower ε_r is required. Irrespective of the frequencies used and the ε_r required, microwave dielectrics require

View Article Online
DOI: 10.1039/C8TC02260G

high *Qf* and near-zero *TCF*.

In this contribution, we critically review the current state of the art in the development of $BiVO_4$ based compositions for potential use in RF applications in the context of current (4G) and future (5G) technology. This is particularly relevant as telecommunication moves in the next 10-20 years from cm to mm wave applications. This revolution will require new materials including much lower loss dielectrics for LTCC technology that can operate at >10 GHz. The review will consider A site substitution, A site defect type, B site substitution, A/B site complex substitutions and composite ceramics of the three polymorphs of $BiVO_4$, summarizing how these modifications improve microwave dielectric properties for future RF applications.

2. Crystal chemistry, synthesis and phase transitions of pure $BiVO_4$

2.1 Orthorhombic phase (Pucherite)

Pucherite $BiVO_4$ was named after the actual Puchermine shaft in the Schneeberg District of Saxony, Germany, where the first specimens were found. It has a yellow brown color with a calculated density ~ 6.69 g/cm^3 as shown in Fig. 1.[35-37] The structure of pucherite $BiVO_4$ was first studied by DeJong and Delange in 1936[1] and determined by Qurashi and Barnes,[2,3] using visually estimated intensities for three principal zones and Buerger procession photographs for data collection. The pucherite $BiVO_4$ structure has a space group Pnca (No. 60) with a = 5.332(5) Å, b = 5.060(5) Å and c = 12.020(5) Å. The crystal structure (Figure 1) is composed of VO_4 tetrahedra and BiO_8 dodecahedra chains, in which slightly distorted VO_4 tetrahedra (two pairs of

View Article Online
DOI: 10.1039/C8TC02260G

bond lengths (1.679(6) Å and 1.803(7) Å) share one edge with the BiO_8 triangulated dodecahedra. BiO_8 dodecahedra share edges with neighboring dodecahedra forming infinite chains. However, attempts to synthesize pucherite by Roth and Waring[4] led to the formation of the monoclinic scheelite phase of $BiVO_4$ and they suggested that pucherite $BiVO_4$ is metastable and only forms under slightly reducing conditions. Moreover, common minor impurities of other phases often co-exist in pucherite $BiVO_4$ which also affect its stability with respect to scheelite. Nonetheless, pucherite $BiVO_4$ has not to date been synthesized in the laboratory and thus there has been no report of its dielectric properties. Due to the limited resource in nature, the microwave dielectric properties of pucherite $BiVO_4$ materials are likely to remain unknown in the near future.

2.2 Zircon phase (Dreyerite)

Zircon-structured $BiVO_4$ also exists in nature as dreyerite named after Gerhard Dreyer, who first discovered the mineral near Kaiserlautern (Germany) where it occurs in rhyolitic tuffs.[38] The crystal structure of dreyerite $BiVO_4$ belongs to a tetragonal zircon family with space group $I4_1/amd$, cell parameters a = 7.303 (3) Å and c = 6.584(3) Å and a calculated density ~ 6.13 g/cm^3.[15,39,40] This structure is composed of slightly distorted BiO_8 dodecahedra (two Bi-O distances, 2.4142 Å and 2.5489 Å) and regular VO_4 tetrahedron (V-O distance ~1.7026 Å) as shown in Fig. 2. In the laboratory, zircon-structured $BiVO_4$ is synthesized by mixing NH_4VO_3 or sodium meta vanadate and $Bi(NO_3)_3*5H_2O$ solutions at room temperature. Zircon-structured $BiVO_4$ has a band gap 2.9 eV in the ultraviolet region.[5,39-41] Zircon-structured $BiVO_4$ irreversibly transforms to monoclinic scheelite at 670-770 K,[42] a transition that is accelerated through mechanical grinding.[43] Many zircon

View Article Online
DOI: 10.1039/C8TC02260G

structured materials have been reported with good microwave dielectric properties, such as $LnVO_4$ (Ln = Nd, Sm etc.). Hence, the zircon $BiVO_4$ might be promising for microwave dielectric applications but its structural instability remains a problem.

2.3 Scheelite monoclinic phase (Clinobisvanite)

Clinobisvanite $BiVO_4$ was first discovered from a pegmatite near Yinnietharra Station.[44] It usually occurs as an accessory mineral in pegmatites formed by the oxidation other bismuth minerals. Clinobisvanite $BiVO_4$ is synthesized by heating mixture of Bi_2O_3 and V_2O_5 above 700 ^oC (Roth and Waring, 1963[4]) and with a = 5.186 Å, b = 11.692 Å, c = 5.084 Å and β = 89.61^o. In 1979, large crystals of clinobisvanite $BiVO_4$ were grown by the Czochralski method under 1 atm of flowing O_2 by Sleight et al.[45] Clinobisvanite $BiVO_4$ was found has a slightly distorted scheelite structure with a space group I112/b with a = 5.1956(1) Å, b = 5.0935(1) Å, c = 11.7045(2) Å and γ = 90.383(1) ^{o}. In the monoclinic scheelite structure, the V cation is tetrahedrally coordinated to oxygen with two different bond lengths (1.7010 Å and 1.7604 Å) and the Bi cation is coordinated to eight oxygens with four different bond lengths from eight different VO_4 tetrahedra as shown in Fig. 3. The monoclinic scheelite $BiVO_4$ is ferroelastic at room temperature and reversibly transforms to paraeleastic $BiVO_4$ with a standard tetragonal scheelite structure (space group $I4_1/a$) under high temperature (255^{o}C) or high pressure.[46-48] Sleight *et al.*[45] pointed out that this phase transition may be driven by the lone-pair Bi^{3+} cation due to the recovery of the distorted dodecahedron during the phase transition and to a lesser extent the VO_4 tetrahedra. In addition to high temperature solid state synthesis, monoclinic scheelite $BiVO_4$ may also be prepared by an alkoxide method at 400 K.[49] Among all the four polymorphs, clinobisvanite $BiVO_4$ is the most stable and the only one that possesses

View Article Online
DOI: 10.1039/C8TC02260G

good microwave dielectric properties. Discussions in this review will mainly focus on modifications of clinobisvanite $BiVO_4$ phase.

2.4 Scheelite tetragonal phase

Scheelite tetragonal $BiVO_4$ is not a stable compound and there is no report that it exists in any natural minerals. Since the discovery of the phase transition from monoclinic to tetragonal scheelite in $BiVO_4$, there has been great interest in the crystal structure of tetragonal scheelite $BiVO_4$. In 1979 Pinczuk et al.[11] found that this phase transition is induced by high pressure (> 1.4 GPa) at room temperature. The crystal structure was resolved by Mariathasan *et al.*[46,50] at 1.6 and 4.3 GPa at 23 ^{o}C as belonging to a standard scheelite structure (space group $I4_1/az$) with a = 5.105(1) Å, b = 5.105(1) Å and c = 11.577(1) Å as shown in Fig. 4. They confirmed that the high-pressure structure is the same as the high temperature $BiVO_4$ phase (above 255 ^{o}C). The V-O tetrahedron remains rigid with no significant change in size at high pressure and the consequent Bi-O polyhedral compression is mainly responsible for the reduction of cell volume. Tetragonal scheelite $BiVO_4$ was also reported to be synthesized by stirring the mixture of $Bi(NO_3)_3$ and Na_3VO_4 solutions with pH adjusted using a Na_2CO_3 or $NaHCO_3$ solution.[51] Although it has similar band gap (2.34 eV) to that of monoclinic scheelite $BiVO_4$ (2.41 eV), it does not promote photocatalytic O_2 evolution. The tetragonal scheelite $BiVO_4$ synthesized by soft chemical method is stable in water but transforms to monoclinic in nitric acid. However, scheelite tetragonal $BiVO_4$ ceramic is unstable at high temperature and cannot be used independently as a microwave dielectric material until such time as future dopant strategies resolve this issue.

View Article Online
DOI: 10.1039/C8TC02260G

2.5 Phase transitions between the polymorphs

Zircon $BiVO_4$ was found to irreversibly transform to scheelite monoclinic phase when annealed above 300 ^oC but mechanical grinding may also induce the phase transition at room temperature.[39-43,51] Natural pucherite $BiVO_4$ transforms to a pure scheelite monoclinic phase when heated above 500 ^oC and cooled room temperature in a sealed Pt tube (Roth and Waring[4,52]) but has never been synthesized in the laboratory. From 420 to 500 ^oC, pucherite $BiVO_4$ coexists with the tetragonal scheelite phase and becomes single phase only above 500 ^oC.[2,3,37,54] Scheelite tetragonal $BiVO_4$ is thus considered metastable and readily transforms to the monoclinic phase in acid solutions.[53] The scheelite monoclinic to tetragonal $BiVO_4$ phase transition is second order at 255 ^oC accompanied by recovery of the distorted BiO_8 dodecahedra and VO_4 tetrahedra to regular polyhedral. This transition may also be induced by external pressure.[53,54] The phase transition sequence of the four polymorphs of $BiVO_4$ is presented in Fig. 5. The complex phase transitions between the four polymorphs of $BiVO_4$, suggest that scheelite monoclinic $BiVO_4$ may be a superior potential MW material due to its structural stability.

3. Crystal structures and dielectric properties of modified $BiVO_4$ materials

Recent progress in the improvement of sintering and microwave dielectric properties of $BiVO_4$ ceramics through A or B site substitutions have suggested that they may be strong candidates for dielectric resonators and as low temperature co-fired ceramics (LTCC).[32,55-57] Dielectric properties of single crystal $BiVO_4$,

View Article Online
DOI: 10.1039/C8TC02260G

obtained from melting Bi_2O_3 and V_2O_5, were first reported by Dudnik et al. in 1974.[6] A twin domain structure is observed in polarizing microscopy which may be removed by applied stress and heating to 230 ^oC. An inflection was observed at 230 ^oC in ε_r vs. temperature in the frequency range 1.5 MHz ~ 10 MHz which was attributed to a ferroelastic phase transition. Bierlein and Sleight[7] confirmed that the scheelite monoclinic to tetragonal $BiVO_4$ phase transition is second order at 255 ± 2 ^oC using *in-situ* optical microscopy and XRD and additionally suggested that it is displacive.

LTCC technology requires materials with $10 \leq \varepsilon_r \leq 100$, $Qf > 5{,}000$ GHz, $TCF < \pm$ 15 ppm/^oC.[30,31] Many low ε_r materials for LTCC technology have been developed and several are commercially available through companies such as Ferro and Dupont.[58,59] However, materials with ε_r above 70 are rare. The $BaO–RE_2O_3–TiO_2$ (RE = La, Nd and Sm) family of MW dielectric ceramics have $\varepsilon_r > 70$ but sinter at > 1200 ^oC.[60,61] If its sintering temperature is lowered to ~ 900 ^oC by glass frits, ε_r decreases to <70 and Qf deteriorates to < 5,000 GHz. The $CaO-Li_2O-Ln_2O_3-TiO_2$ family of MW dielectrics has a high sintering temperature but low Qf.[62] Some Pb-based temperature stable MW dielectrics also exhibit large ε_r but[63] due to their toxicity have been gradually phased out. As reported by Roth and Waring[4] and confirmed by Bierlein and Sleight,[7] $BiVO_4$ melts congruently at 940 ^oC, lower than the melting point of silver (961 ^oC) which suggest it may be viable for LTCC technology. However, Valant and Suvorov[28] reported that although $BiVO_4$ possessed attractive microwave dielectric properties, it reacted seriously with silver at its sintering temperature forming $Bi_3AgV_2O_{10}$, as shown in Fig. 6 and was thus unsuitable for LTCC applications. However, although $BiVO_4$ reacts with silver, its low sintering temperature, high ε_r and Qf are still attractive if the poor compatibility with Ag electrodes can be solved. In 2010, we reported that[32] the introduction of 10 mol. % $(Li_{0.5}Bi_{0.5})MoO_4$ into $BiVO_4$ lowered its

View Article Online
DOI: 10.1039/C8TC02260G

sintering temperature to > 660 ^{o}C with an increase in ε_r and *Qf* to 81 and 8,000 GHz, respectively. $BiVO_4$-$(Li_{0.5}Bi_{0.5})MoO_4$ ceramics are chemically compatible with Al and Cu but not Ag electrodes. Subsequently, a series of modifications of $BiVO_4$ ceramics using solid solution or composite approaches increased ε_r, improved *Qf* and modified TCF.[55-57,64,65] In the following section, the phase evolution, crystal structure and microwave dielectric properties of $BiVO_4$ modifications are discussed and put into wider context.

3.1 A site substitution type

3.1.1 Lanthanum series substitution $(Bi_{1-x}Ln_x)VO_4$ (Ln = Lanthanum and Y)

Among all the lanthanides, La^{3+} has the largest ionic radius (1.16 Å for CN = 8) closest to that of Bi^{3+} (1.17 Å).[66] Hence, La^{3+} is the most promising substituent for Bi^{3+} in $BiVO_4$. Lanthanum orthovanadate was reported to crystallize in two polymorphs, monazite-type monoclinic and zircon-type tetragonal phases with the latter is metastable.[67-71] In the study of Kwolek *et al.*,[72] $(Bi_xLa_{1-x})VO_4$ materials were obtained via a microwave-assisted hydrothermal route. The monoclinic $BiVO_4$, zircon and monazite phases coexisted at x = 0.07, which indicated that La does not substitute for Bi in monoclinic $BiVO_4$ during hydrothermal processing. However, in Kwolek et al.'s work,[72] all the $(Bi_xLa_{1-x})VO_4$ materials were synthesized at < 300 ^{o}C with no further high temperature treatments.

Dragomir *et al.*[73] found that for x > 0.08 in the $(Bi_{1-x}Nd_x)VO_4$ solid solution, peaks from a secondary zircon-type $(Nd,Bi)VO_4$ phase are present in XRD traces, Fig. 7. For ≤ 0.05, no peaks of zircon-type $(Nd,Bi)VO_4$ phase were observed and further

View Article Online
DOI: 10.1039/C8TC02260G

surmised that Nd cannot occupy the Bi site in monoclinic $BiVO_4$ from Extended X-ray Absorption Fine Structure (EXAFS) data, from which large differences in the neighboring environment of Bi and Nd ions were detected.

Based on their study, Dragomir et al.[73] concluded that a composite region of monoclinic $BiVO_4$ and $Bi_{0.49}Nd_{0.51}VO_4$ exists for $0<x<0.51$ and a zircon-type $(Nd,Bi)VO_4$ solid solution is formed for $0.51\leq x\leq 1$, and therefore Nd stabilizes the zircon-type $BiVO_4$ phase. However, no dielectric properties were reported.

In the $(Bi_{1-x}Ce_x)VO_4$ system[74] weak peaks of zircon-type phase existed in XRD patterns of powders with x = 0.1 calcined 4 h at 650 ^oC but disappeared in samples sintered 2 h at 780 ^oC, as shown in Fig. 8. Similarly, the heat treatment temperature effects the phase equilibrium for $0.1<x<0.6$, as shown in Fig. 8. Finally, a monoclinic $(Bi,Ce)VO_4$ solid solution formed for $x\leq 0.1$, a composite region containing both monoclinic $(Bi_{0.9}Ce_{0.1})VO_4$ and zircon-type $(Bi_{0.4}Ce_{0.6})VO_4$ for $0.1<x\leq 0.6$ and a zircon-type $(Bi,Ce)VO_4$ solid solution for $0.6<x\leq 1$. However, EXAFS data were not available to support the conclusion that Ce can enter the Bi site in monoclinic $BiVO_4$. If Ce only enters the Bi site of the zircon phase, i.e. a $(Bi_{0.9}Ce_{0.1})VO_4$ sample is a composite of $BiVO_4$ and $(Bi_{0.4}Ce_{0.6})VO_4$, then the phase transition temperature of $(Bi_{0.9}Ce_{0.1})VO_4$ sample should be the same as $BiVO_4$ (~ 255 ^oC). Our data however, revealed (Fig. 9), that the phase transition temperature of $(Bi_{0.9}Ce_{0.1})VO_4$ from thermal expansion data is ~ 160 ^oC, a result which, if correct, overturns the above assumption and supports a greater level of solid solubility of Ce for Bi in monoclinic $BiVO_4$. We note however, that the ferroelastic transition is susceptible to external stress which may influence its onset temperature.

ε_r of the $(Bi_{1-x}Ce_x)VO_4$ ceramics decreased almost linearly with the increase in x while Qf increased. The microwave dielectric properties of zircon-structured $CeVO_4$

View Article Online
DOI: 10.1039/C8TC02260G

were reported by Zuo *et al.*[75] with ε_r ~ 12.3, *Qf* ~ 41,460 GHz, and *TCF* ~ − 34.4 ppm/^{o}C. Zircon-structured $(Bi_{0.4}Ce_{0.6})VO_4$ has *TCF* = + 173 ppm/^{o}C and thus there are two possibilities to design temperature stable microwave dielectrics: $(Bi_{0.9}Ce_{0.1})VO_4$-$(Bi_{0.4}Ce_{0.6})VO_4$ composites (monoclinic and tetragonal phases) and $(Bi_{1-x}Ce_x)VO_4$ solid solutions.

In the work of Neves *et al.*,[76] $(Bi_{1-x}Ce_x)VO_4$ films showed a red shift of the optical band edge and a decrease of the reflectance as Ce^{3+} concentration increases which may also relate to the substitution of Ce for Bi in the monoclinic scheelite structure. In the work of Xu *et al.*,[77] 8 mol. % La^{3+}, Ce^{3+}, Gd^{3+}, Yb^{3+}, Eu^{3+}, Ho^{3+}, Nd^{3+} and Sm^{3+} ions were substituted for Bi in $BiVO_4$. From their XRD data, only Gd^{3+} and Yb^{3+} doped samples show peaks from secondary phases but changes of the cell parameters in the doped samples, not considered by the authors should have indicated unambiguous evidence of solid solution and they incorrectly concluded that RE ions do not enter the $BiVO_4$ lattice.

In the contribution of Wang et al.[78], Dy^{3+} entered the Bi^{3+} site and composites of monoclinic scheelite and zircon phases were obtained in the $(Bi_{1-x}Dy_x)VO_4$ system prepared via solid state reaction method in the range $0.1 \leq x \leq 0.2$, as shown in Fig. 10. The data from Wang *et al.* contradicted results from $(Bi_{0.9}Ce_{0.1})VO_4$, which indicates that it becomes difficult for smaller Ln ions (1.027 Å for Dy^{3+}) to occupy the A site in $BiVO_4$. Pure zircon solid solution was reported to form when $x \geq 0.3$. Wang *et al.* also studied the $(Bi_{0.5}M_{0.5})VO_4$ (M = La, Sm, Nd, Gd, Eu, and Y) compositions and only zircon solid solutions were formed after calcinations at 850 ^{o}C, which means that Ln rich compositions prefer to crystallize in the zircon phase.

Y has the similar physical and chemical properties to the lanthanides but with a smaller ionic radius (1.019 Å) and in many systems it replaces or substitutes for Ln

View Article Online
DOI: 10.1039/C8TC02260G

ions. As shown in Fig. 11, $(Bi_{1-x}Y_x)VO_4$ ceramics are composed of monoclinic scheelite $BiVO_4$ and tetragonal zircon-type $(Bi_{0.6}Y_{0.4})VO_4$ phases for $x < 0.4$.[79,80] Hence, there is no evidence that Y enters the A site of monoclinic $BiVO_4$. We note that high temperature promotes the formation of the zircon-type phase in $(Bi_{1-x}Y_x)VO_4$ ceramics ($0.10 \leq x \leq 0.65$) and its concentration was higher in sintered than calcined samples. For $x \geq 0.4$, a zircon-type solid solution was formed and cell parameters decreased linearly with Y concentration. Pure YVO_4 has $\varepsilon_r \sim 11$, $Qf \sim 28{,}600$ GHz, TCF ~ − 61.3 ppm/°C and sinters at > 1550 °C, as shown in Fig. 12. Hence, both end members in the $(Bi_{1-x}Y_x)VO_4$ system have negative *TCF*. Similar to the $(Bi_{1-x}Ce_x)VO_4$ system, Bi also plays an important role in *TCF* of the $(Bi_{1-x}Y_x)VO_4$ zircon-type solid solution. With increase of Bi concentration in zircon $(Bi,Y)VO_4$ ceramics, *TCF* shifted from negative to positive, leading to two temperature stable compositions: $(Bi_{0.81}Y_{0.19})VO_4$ composite ceramic sintered at 870 °C ($\varepsilon_r \sim 45$, $Qf \sim 14{,}000$ GHz and TCF + 10 ppm/°C) and a $(Bi_{0.2}Y_{0.8})VO_4$ solid solution sintered at 1075 °C ($\varepsilon_r \sim 16.3$, $Qf \sim 31{,}100$ GHz and TCF ~ – 11.9 ppm/°C), as shown in Fig. 12.

Although only limited data on the $(Bi_{1-x}A_x)VO_4$ systems have been reported, a rough phase composition diagram (room temperature) of $(Bi_{1-x}A_x)VO_4$ ceramics as a function of A ionic radius is shown in Fig. 13.[61-83] Among the lanthanides, although La^{3+} has a similar ionic radius to Bi^{3+}, $LaVO_4$ prepared via solid state synthesis densifies at ~ 850 °C and crystallizes in a monoclinic monazite structure with a ε_r = 14.2, Qf = 48197 GHz and *TCF* = − 37.9 ppm/°C. In addition, Wang *et al.*[78] reported that a zircon solid solution formed for $(Bi_{0.5}La_{0.5})VO_4$ at 850 °C.

Based on the existing evidence, five possible distinct regions are proposed to exist in the $BiVO_4$-$LnVO_4$ system. As the ionic radius of the Ln ion decreases, it becomes more difficult to retain a monoclinic $BiVO_4$ solid solution and easier to form $LnVO_4$

View Article Online
DOI: 10.1039/C8TC02260G

zircon solid solutions. A schematic of the trends in phase compositions are summarized in Fig. 13 based on the available experimental data. All zircon-structured $LnVO_4$ ceramics have –ve *TCF*. Bi substitution increases ε_r shifting *TCF* positive. Hence, in $BiVO_4$-$LnVO_4$ ceramics, we anticipate two compositions with near-zero TCF: a $(Ln,Bi)VO_4$ solid solution and a $BiVO_4$-$(Ln,Bi)VO_4$ composite, as illustrated in Fig. 13. For monoclinic $(Bi,Ln)VO_4$ solid solution region, a maximum ε_r is achieved at the phase boundary composition. For lanthanides with ionic radius smaller than Nd^{3+}, ε_r of monoclinic $BiVO_4$-$LnVO_4$ ceramics decreases linearly with increase of Ln concentration with compositions exhibiting *Qf*>5,000 GHz.

3.1.2 Other trivalent species:Fe^{3+}, In^{3+}, Sc^{3+} and Ga^{3+}

Agunaou *et al.*[84] studied the substitution of Gd^{3+} for Bi^{3+} in the $(Bi_xGd_{1-x})VO_4$ prepared via a co-precipitation route. A zircon-type solid solution was formed in the range $0 \leq x \leq 0.3$ and a scheelite solid solution (presumably tetragonal) was formed in the range $0.3 \leq x \leq 0.64$. However, no further compositions with $x > 0.64$ were studied. Yeom *et al.*[85] employed Electron Paramagnetic Resonance (EPR) to confirm that Gd^{3+} substitutes for Bi^{3+} in monoclinic $BiVO_4$ but no further data on the ceramics was reported. Yin *et al.*[86] studied the composite of In_2O_3-$BiVO_4$ by using a soft chemical approach with composites sintered at 500 ^oC. When the In/Bi ratio was less than unity, only monoclinic $BiVO_4$ phase was detected using XRD, as shown in Fig. 14, which indicated that monoclinic $(Bi,In)VO_4$ solid solution might be formed over a wide compositional range. Fe^{3+} has an ionic radius of 0.78 Å (CN = 8) and 0.49Å (CN = 4) and prefers to reside on the B site in $BiVO_4$. In our previous work on $(Bi_{1-x}Fe_x)VO_4$ ($x \leq 0.40$)[87] for $x \leq 0.08$, no secondary phases were revealed in XRD patterns but for $x > 0.08$ peaks of $FeVO_4$ phase were observed. However, the phase transition

View Article Online
DOI: 10.1039/C8TC02260G

temperatures were independent of Fe content at 255 ^{o}C, as shown in Fig. 15, which indicated that Fe did not occupy the A site in monoclinic $BiVO_4$. Pure $FeVO_4$ was found to crystallize in a triclinic structure with space group number P-1,[88] in which Fe is 6-coordinated. It was concluded that Fe^{3+} with CN = 8 is too small to substitute for Bi^{3+} in $BiVO_4$.

3.2 B site substitution type

3.2.1 Single pentavalent ions substitutions (Nb^{5+}, Ta^{5+}, Sb^{5+} and P^{5+})

The ionic radius of V^{5+} in monoclinic $BiVO_4$ is 0.355 Å with CN = 4. Both $BiNbO_4$ and $BiTaO_4$ crystallize in an orthorhombic structure, in which Nb and Ta prefer to be in 6-rather than 4 coordinated[89,90] polyhedra due to their large radius (0.48 for CN = 4). This preference poses potential limitations and the ability of Nb and Ta to substitute for V in monoclinic $BiVO_4$. In the study of Monfort et al.,[91] Nb-modified $BiVO_4$ films were prepared via a sol-gel technique, XRD patterns from which suggested that Nb doping leads to merging of (200) and (020) peaks, which is strongly related with the transition from the monoclinic to tetragonal scheelite structure, suggesting Nb may enter the V site in monoclinic $BiVO_4$. In addition, Zhao et al.[92] pointed out that Nb substitution for V is thermodynamically feasible but broadly speaking its solid solubility in monoclinic $BiVO_4$ is unknown. Kumari et al.[93] prepared a series of $Bi(V_{1-x}Ta_x)O_4$ and $Bi(V_{1-x}P_x)O_4$ samples via solid state reaction method and found that only mixed phases were observed, implying Ta^{5+} and P^{5+} cannot occupy the V site in monoclinic $BiVO_4$. However, Loiudice et al.[94] reported the substitution of Sb^{5+} for V^{5+} in monoclinic $BiVO_4$ lattice by both structural characterization and first principles calculations but irrespective of the solid solubility

View Article Online
DOI: 10.1039/C8TC02260G

of single pentavalent ions there have been no reports of their effect on the microwave dielectric properties of $BiVO_4$ ceramics.

3.2.2 Complex pentavalent ions substitutions ($Fe_{1/3}Mo_{2/3}$), ($In_{1/3}Mo_{2/3}$), ($Sc_{1/3}Mo_{2/3}$), ($Ga_{1/3}Mo_{2/3}$) and ($Ge_{1/2}Mo_{1/2}$)

The $Bi(Fe_{1/3}Mo_{2/3})O_4$ phase was first synthesized by Sleight and Jeitschko in 1974[95] and was the first example of a trivalent cation on the tetrahedral sites of the $CaWO_4$ type tetragonal scheelite structure, in which FeO_4 and MoO_4 tetrahedra are ordered. Similarly, an ordered scheelite structure also formed in $Bi(Ga_{1/3}Mo_{2/3})O_4$, $Bi(In_{1/3}Mo_{2/3})O_4$ and $Bi(Sc_{1/3}Mo_{2/3})O_4$, whereas compounds with Al and Cr as the trivalent species are unstable in ambient conditions[95-98] since the latter favor CN4 rather than CN = 6 coordination. We note that $Bi(Ge_{1/2}Mo_{1/2})O_4$ has not been studied but may form the ordered scheelite structure since Ge has a similar effective ionic radius (0.39 Å) in CN = 4 to V^{5+} and Mo^{6+}.

Given the above knowledge of crystal chemistry of complex pentavalent site compounds, it is reasonable to propose that ($Fe_{1/3}Mo_{2/3}$), ($In_{1/3}Mo_{2/3}$), ($Sc_{1/3}Mo_{2/3}$), ($Ga_{1/3}Mo_{2/3}$) and ($Ge_{1/2}Mo_{1/2}$) substitute for V^{5+} in $BiVO_4$. Only the $xBi(Fe_{1/3}Mo_{2/3})O_4$–$(1-x)BiVO_4$ ($0.0 \leq x \leq 1.0$) system has been studied to date.[56] For $0.0 \leq x < 0.10$, a scheelite monoclinic solid solution formed, as shown in Fig. 16. As x increased to 0.70, a scheelite tetragonal solid solution is stable but for $0.70 \leq x < 0.90$, a composite region containing scheelite tetragonal and scheelite-distorted $Bi(Fe_{1/3}Mo_{2/3})O_4$ type monoclinic phases was revealed. Finally, a $Bi(Fe_{1/3}Mo_{2/3})O_4$ type monoclinic solid solution is formed in the range $0.90 \leq x \leq 1.00$. The phase transition temperatures from scheelite monoclinic to tetragonal structure for $x \leq 1.0$ samples are easily obtained from the thermal expansion data as shown in Fig. 17 in

View Article Online
DOI: 10.1039/C8TC02260G

which there is a sudden increase of thermal expansion coefficient from below + 5 ppm/^{o}C to above + 12 ppm/^{o}C, related to monoclinic and tetragonal phases, respectively. As x increases from 0 to 0.10, the phase transition temperature decreases linearly from 255 ^{o}C to ~ − 9 ^{o}C, similar to the trend of T_C vs. external pressure reported by Hazen and Mariathasan,[46] Fig. 18. The continuous phase transition induced by substitution of ($Fe_{1/3}Mo_{2/3}$) for V is attributed to the increase in internal pressure due to the increase in atomic packing factor within the monoclinic phase region, which is related to the minimum cell parameter at x = 0.1.

ε_r and *Qf* reached maximum values of 74.8 and 11,600 GHz, respectively, at the phase boundary composition x = 0.1 which we propose is related to the minimum cell volume and maximum atomic packing factor at this point in the compositional series, Fig. 19. ε_r = 74.8, *Qf* = 11,500 GHz, accompanied by a *TCF* = +20 ppm/^{o}C over a wide temperature range may also be obtained for composite ceramic sample made from mixture of granulated powders, which is promising for microwave device applications.

Based on the similar ordered crystal structures, we postulate that ($In_{1/3}Mo_{2/3}$), ($Sc_{1/3}Mo_{2/3}$), ($Ga_{1/3}Mo_{2/3}$) and ($Ge_{1/2}Mo_{1/2}$) substitution for V in $BiVO_4$ will give rise to similar trends as for the x$Bi(Fe_{1/3}Mo_{2/3})O_4$–(1-x)$BiVO_4$ system.

3.3 A and B site complex substitution and defect types

3.3.1 (A^+B^{7+}) complex substitutions

$A^+B^{7+}O_4$ (A = Li, Na, K and Ag; B = F, Cl, B, I and Re) compounds also crystallize in the scheelite tetragonal structure suggesting that (A^+B^{7+}) complex substitutions on both A and B sites in $BiVO_4$ might lead to a solid solution. However, to date there are

View Article Online
DOI: 10.1039/C8TC02260G

no reports on any $A^{+}B^{7+}O_4$-$BiVO_4$ compositions. Typically, $A^{+}B^{7+}O_4$ (A = Li, Na and K; B = F, Cl, Br and I) compounds have larger cell parameters than $BiVO_4$ and therefore the formation of a mixture of two scheelite phases is a strong possibility even if the processing difficulties associated with different melting temperatures ($BiVO_4$, 920 ^{o}C) and, e.g., $NaIO_4$ (300 ^{o}C) can be overcome. However, the possibility of using $A^{+}B^{7+}O_4$ compounds as sintering aids to further reduce the processing temperatures of scheelite structured compounds perhaps should be explored.

3.3.2 ($A^{2+}B^{6+}$) complex substitutions (A = Ca, Ba, Sr, Cd, Pb, ($Li_{0.5}Bi_{0.5}$), ($Na_{0.5}Bi_{0.5}$), ($K_{0.5}Bi_{0.5}$), ($Ag_{0.5}Bi_{0.5}$), ($Li_{0.5}Ln_{0.5}$), ($Na_{0.5}Ln_{0.5}$); B = Mo, W, Cr)

A = Ca, Ba, Sr, Cd, Pb etc.; B = Mo, W, Cr.

The scheelite structure was named after the chemist Carl Wilhelm Scheele, who first discovered the mineral scheelite, $CaWO_4$.[99,100] The scheelite structure is adaptable with bivalent ions, such as Ca^{2+}, Ba^{2+}, Sr^{2+} and Cd^{2+}, occupying the A site and hexavalent species, such as Mo^{6+}, W^{6+} and Cr^{6+}, the B-site. Most of $AMoO_4$ and AWO_4 ceramics possess low ε_r between 7 ~ 17, Qf > 30,000 GHz and negative TCF ~ − 60 ppm/°C.[101-103] Hence, they are compatible with $BiVO_4$ ceramics. In 2006, Yao and Ye[104] reported a complete scheelite solid solution for $(Ca_xBi_{1-x})(V_{1-x}Mo_x)O_4$. The phase transition from monoclinic to tetragonal occurred at x = 0.1, similar to $xBi(Fe_{1/3}Mo_{2/3})O_4$–(1-x)$BiVO_4$ discussed above.[56] However, Yao and Ye[104] did not study in detail compositions with x<0.1. Sameera *et al.*[105] confirmed the findings of Yao and Ye[106] who later reported that 50 mol.% of $CaWO_4$ with $BiVO_4$ resulted in formation of scheelite tetragonal solid solution. Sameera *et al.*[107] subsequently confirmed the formation of a scheelite tetragonal solid solution in

View Article Online
DOI: 10.1039/C8TC02260G

$(Bi_xCa_{1-x})(V_xW_{1-x})O_4$ ($0.2 \le x \le 0.8$). The microwave dielectric properties of the $(Bi_xCa_{1-x})(V_xW_{1-x})O_4$ ($0.1 \le x \le 0.5$) ceramics were studied by Ding and Bian in 2013[108] who reported with $\varepsilon_r \sim 22.1$, $Qf \sim 16{,}730$ GHz ($f = 8.08$GHz) and $TCF = -2.4$ ppm/^oC for x = 0.3 sintered 2 h at 950 ^oC. Although both of the end members possess negative TCF, near zero TCF is achieved within the solid solution due to the phase transition from monoclinic to tetragonal scheelite.

A=($Li_{0.5}Bi_{0.5}$), ($Na_{0.5}Bi_{0.5}$), ($K_{0.5}Bi_{0.5}$), ($Ag_{0.5}Bi_{0.5}$), ($Li_{0.5}Ln_{0.5}$), ($Na_{0.5}Ln_{0.5}$); B=Mo, W, Cr

Most of $(A^+_{0.5}B^{3+}_{0.5})X^{6+}O_4$ (A^+ = Li, Na, K, Rb, Cs and Ag; B = Bi^{3+} and Ln^{3+}; X = Mo^{6+}, W^{6+} and Cr^{6+}) materials crystallize in the scheelite tetragonal or related ordered structures and some possess good microwave dielectric properties (see Table 1).[109-122] Among them, the $(Na^+_{0.5}Ln_{0.5})X^{6+}O_4$ ceramics have similar microwave dielectric properties to $AMoO_4$ and AWO_4 ceramics, while the $(Li^+_{0.5}B^{3+}_{0.5})X^{6+}O_4$ ceramics have a –ve TCF with $\varepsilon_r > 20$.[113-115] Hence, some are good candidates to substitute in $BiVO_4$ to modify its microwave dielectric properties. For the compositional series $(1\text{-}x)BiVO_4\text{-}x(Li_{0.5}Bi_{0.5})MoO_4$,[32] $(Li_{0.5}Bi_{0.5})MoO_4$ ceramic sinters at 550 ^oC with $\varepsilon_r \sim 44.4$, $Qf \sim 3{,}200$ GHz, and TCF ~ + 245 ppm/^oC.[123] A scheelite monoclinic solid solution forms for $0 \le x \le 0.10$ and a scheelite tetragonal solid solution for $0.1 < x \le 1.0$.[32] As x increased in the $(1\text{-}x)BiVO_4\text{-}x(Li_{0.5}Bi_{0.5})MoO_4$ series, the cell parameter *a* decreased and *b* increased, becoming equal at x = 0.10 with the *c* axis decreasing monotonously. This resulted in a minimum cell volume at x = 0.1, as shown in Fig. 20. When x > 0.1, both *a* and *c* increased linearly due to the larger ionic radius of Mo^{6+} in comparison with V^{5+}. A comparison of cell parameters between the $(1\text{-}x)BiVO_4\text{-}x(Li_{0.5}Bi_{0.5})MoO_4$ and $BiVO_4$ as a function of x, temperature and pressure is presented in Fig. 20. The increase in "internal pressure" caused by substitution by a

View Article Online
DOI: 10.1039/C8TC02260G

B-site ion of larger radius results in a similar effect on the crystal structure as the application of external pressure and temperature. The net result is lowering of the phase transition from 255 ^{o}C for $BiVO_4$ to near room temperature for x = 0.1. In this system, the phase transition from monoclinic to tetragonal phase were first observed[124] from microwave dielectric spectroscopy, as shown in Fig. 21. According to the classic Lyddane–Sach–Teller relation,[125] there is usually a maximum value of permittivity observed at the ferroelastic phase transition temperature if there is a coupling to an optic mode, as is the case here. In fact, this method only works at very high frequency (above 1 MHz) in this system and the peaks in ε_r are usually obscured due to the high conductivity at low frequency. *In-situ* XRD, Raman and Far infrared reflection spectroscopy can also be employed to determine the phase transition temperature. As shown in Fig. 22 and Fig. 23,[126] as temperature increased, characteristic XRD peaks (200) and (020) merge into one peak gradually, caused by convergence of *a* and *b* lattice parameters in monoclinic structure. Similarly, the symmetric A_g bending mode of the vanadate anion $\delta_s(VO_4)$ and the anti-symmetric B_g bending mode of the vanadate anion $\delta_{as}(VO_4)$ at 357.2 and 327.4 cm^{-1}, respectively, merged into one mode gradually at the phase transition temperature because the λ_1 and λ_2 of V-O bond lengths approach and finally became equal. Merging of reflection peaks are also observed in *in-situ* far infrared spectroscopy, as shown in Fig. 23 but ε_r of this system is dominated by overlapping external modes below 200 cm^{-1} related with Bi^{3+}. Hence, it is difficult to accurately determine the intrinsic ε_r as a function of temperature.

A maximum value of ε_r is obtained at the phase boundary (x = 0.1) which is attributed to the minimum cell volume. The trend in ε_r is almost inverse to that of cell volume vs. composition because molecular polarization is determined by the cell

View Article Online
DOI: 10.1039/C8TC02260G

volume and ionic polarizability. *Qf* remains high (> 8,000 GHz) in the monoclinic solid solution region and then decreases with composition in the tetragonal phase region, consistent with larger atomic packing factor within the monoclinic structure than the tetragonal. Third, TCF values were affected dramatically by the phase transition temperature. Conventionally, the resonant frequencies at 25 ^{o}C and 85 ^{o}C are used to calculate TCF. Hence, if a phase transition temperature is > 85 ^{o}C, a large –ve TCF is obtained. When a phase transition temperature is < 25 ^{o}C, a large +ve TCF is obtained. For samples in which the phase transition temperature lies between 25 ~ 85 ^{o}C, the resonant frequency is nonlinear and large deviations in TCF are observed.

Similar results were further obtained for (1-x)$BiVO_4$-x$(Na_{0.5}Bi_{0.5})MoO_4$ and (1-x)$BiVO_4$-x$(Ag_{0.5}Bi_{0.5})MoO_4$ systems.[55,64] For some other end member with ordered or modified structures rather than tetragonal scheelite, such as $(K_{0.5}Bi_{0.5})MoO_4$ and $(Li_{0.5}La_{0.5})MoO_4$ which crystallize in an A site ordered monoclinic phase and an orthorhombic structure with a Pbca space group, respectively,[127-131] similar phase transition are also obtained within a limited solid solubility. For example, for (1-x)$BiVO_4$-x$(K_{0.5}Bi_{0.5})MoO_4$ ceramics,[57] the phase diagram can be separated into at least six regions below the melting point, as shown in Fig. 24: Region I, scheelite monoclinic phase ($BiVO_4$ type) from $0 \leq x < 0.1$; Region II, scheelite tetragonal phase ($BiVO_4$ type) for $0.1 \leq x < 0.19$; Region III, two scheelite tetragonal phases (o-$BiVO_4$ and t-$(KBi)_{1/2}MoO_4$ type) for $0.1 \leq x < 0.82$; Region IV, scheelite tetragonal phase solid solution from $0.82 \leq x \leq 0.85$ ($(KBi)_{1/2}MoO_4$ type); Region V, composite phase from $0.85 < x < 0.88$ ($(KBi)_{1/2}MoO_4$ type tetragonal and monoclinic phases) and VI, scheelite monoclinic phase ($(KBi)_{1/2}MoO_4$ type) from $0.91 \leq x \leq 1.0$. Hence, it is concluded that provided one end member, $(A^{+}_{0.5}A^{3+}_{0.5})B^{6+}O_4$, has a scheelite related structure, the substituent ions may reside within $BiVO_4$ lattice and form a solid

View Article Online
DOI: 10.1039/C8TC02260G

solution, in which the monoclinic to tetragonal phase occurs at a composition with minimum cell parameters and largest atomic packing factor.

All Li rare earth double molybdates crystallize in a classic scheelite structure except $(LiLa)_{0.5}MoO_4$ is orthorhombic.[132,133] Li rare earth double molybdates readily form solid solution with monoclinic $BiVO_4$. Sameera *et al.*[130] synthesized $(Li_{0.5x}La_{0.5x}Bi_{1-x})(Mo_xV_{1-x})O_4$ compositions by solid state reaction from $0 \leq x \leq 0.5$ and a complete scheelite solid solution was formed. Although they didn't give the precise phase boundary composition between monoclinic and tetragonal phases, the monoclinic solid solubility is expected at ~10 % with a classic scheelite solid solution for $0.1 \leq x \leq 0.5$. However, un-doped $(Li,La)_{0.5}MoO_4$ crystallizes in an orthorhombic structure. Hence, there should be a limited region for scheelite solid solution. Subsequently, Sameera *et al.*[131] reported other similar systems such as $(Li_{0.1}Ln_{0.1}Bi_{0.8})(Mo_{0.2}V_{0.8})O_4$ (Ln = La, Pr, Sm, Gd, Tb, Dy, Y, Yb and Lu) and found that a scheelite solid solution is formed for Ln = La, Pr, Sm, and Gd, and that cell volume decreases with the decrease in rare earth ionic radius. When ionic radius decreases to 1.04 Å for Ln = Tb, zircon as a secondary phase as revealed from the XRD data shown in Fig. 25, which indicates that small Ln ions have a tendency to prefer the $LnVO_4$ zircon rather than scheelite phase.

For the $(Li_{0.5}Ln_{0.5})WO_4$ system, compositions with ionic radius large than Gd^{3+} crystallize in the scheelite structure but only $(Li_{0.5}Sm_{0.5})WO_4$ and $(Li_{0.5}Nd_{0.5})WO_4$ are reported as microwave dielectrics.[120,121,134,135] Chen et al.[136,137] studied the microwave dielectric properties of $(1-x)BiVO_4$-$x(Li_{0.5}Sm_{0.5})MoO_4$ and $(1-x)BiVO_4$-$x(Li_{0.5}Nd_{0.5})MoO_4$ systems and obtained $\varepsilon_r > 75$ and $Qf > 6{,}000$ GHz. However, there was no discussion of the large non-linear deviation of resonant frequency as a function of temperature.

View Article Online
DOI: 10.1039/C8TC02260G

Due to the existence of many $A^{2+}B^{6+}O_4$ ceramics with good microwave dielectric properties, this series of materials are promising candidates to form solid solutions with $BiVO_4$ ceramics. A phase composition diagram as a function of A-site ionic radius for $AMoO_4$ phases is shown in Fig. 26. For almost all the reported $A^{2+}B^{6+}O_4$-$BiVO_4$ ceramics,[55,108,138] 10 mol. % $A^{2+}B^{6+}O_4$ substitution induces the phase transition from monoclinic $BiVO_4$ to tetragonal. However, there is no other notable relation. For A-site ions with radii in the range 1.045 ~ 1.225 Å (e.g. $(Li_{0.5}Bi_{0.5})^{2+}$, Ca^{2+}, $(Na_{0.5}Bi_{0.5})^{2+}$, $(Ag_{0.5}Bi_{0.5})^{2+}$), the other end members with formula, $A^{2+}MoO_4$, crystallize in a tetragonal scheelite structure and have comparable cell parameters with undoped $BiVO_4$. This leads to a whole range scheelite solid solutions which are monoclinic when the $BiVO_4$ concentration is > 90% and which are tetragonal when the $BiVO_4$ concentration is < 90%. For $(K_{0.5}Bi_{0.5})^{2+}$ complex ions with average radius ~ 1.34 Å, only 20 % scheelite solid solubility was obtained and there are six phase regions revealed by XRD. Even in the undoped $(K_{0.5}Bi_{0.5})MoO_4$ ceramics, the tetragonal scheelite structure does not form and an A site ordered monoclinic structure is preferred. Although $BaMoO_4$ also crystallizes in tetragonal scheelite phase,[139] the large ionic radius at A site may give rise to a more complicated phase assemblage. As with $LaVO_4$ discussed in chapter 3.1.1, the $(Li_{0.5}La_{0.5})MoO_4$ in a unique orthorhombic structure with Pbca symmetry and this may lead to four phase regions as illustrated in Fig. 26. Except for $(Li_{0.5}La_{0.5})MoO_4$, almost all $(Li_{0.5}Ln_{0.5})MoO_4$ ceramics prepared via solid state reaction crystallize in a tetragonal scheelite structure. However, there is no evidence that $BiVO_4$-$(Li_{0.5}Ln_{0.5})MoO_4$ (Ln ≠ La) ceramics form solid solutions across the whole composition range. On the contrary, there is compelling evidence that scheelite solid solubility in $BiVO_4$-$(Li_{0.5}Ln_{0.5})MoO_4$ (L n ≠ La) ceramics decrease with the decrease of $(Li_{0.5}Ln_{0.5})$

View Article Online
DOI: 10.1039/C8TC02260G

($Ln \neq La$) ionic radius. In the ($Li_{0.5}Ln_{0.5}$) ($Ln \neq La$) rich region, zircon $LnVO_4$ phase is detected by the XRD. Hence, in the ($Li_{0.5}Ln_{0.5}$) ($Ln \neq La$) rich region there may be at least three regions: ($Li_{0.5}Ln_{0.5}$)MoO_4 tetragonal phase; ($Li_{0.5}Ln_{0.5}$)MoO_4 + zircon $LnVO_4$ phase and zircon $LnVO_4$ + $BiVO_4$-rich scheelite phase. Due to the absence of reported data, these parts are left blank in Fig. 26. In all $BiVO_4$-$AMoO_4$ ceramics, when the A site ions are larger than 1.04 Å (for $Li_{0.5}La_{0.5}$), the phase transition from monoclinic $BiVO_4$ to tetragonal scheelite phase usually leads to a maximum ε_r at the phase boundary due to the achievement of a minimum value of cell volume which decreases linearly in the single phase regions. When the A site ionic radius decreases below that of La, the decrease in ionic polarizability[140] dominates the trend in ε_r which decreases linearly as a function of Ln content. *Qf* of the $BiVO_4$ rich scheelite solid solutions are expected to be > 5,000 GHz, especially for $BiVO_4$-$CaMoO_4$, $BiVO_4$-($Na_{0.5}Bi_{0.5}$)MoO_4, and $BiVO_4$-($Ag_{0.5}Bi_{0.5}$)MoO_4 ceramics, for which 8,000 GHz can be obtained across the whole composition range. However, due to the phase assemblage and large difference in sintering temperatures between these phases in the $BiVO_4$-($Li_{0.5}Ln_{0.5}$)MoO_4 ($Ln \neq La$) ceramics, poor *Qf* results. Generally, it is difficult to obtain near-zero TCF in simple solid solutions or composite in the ($A_1^+A_2^{3+}$)$B^{6+}O_4$-$BiVO_4$ family. Only layered or large particle composites are effective due to inter-diffusion. According to our recent results,[113-115] most ($Na_{0.5}Ln_{0.5}$)MoO_4 ceramics possess similar ε_r and TCF to that of $AMoO_4$ (A = Ca, Sr, Ba) with *Qf*> 20,000 GHz. Although no work has been carried out to date, we speculate based on generic trends that ($Na_{0.5}Ln_{0.5}$)MoO_4 ceramics might provide near-zero TCF in $BiVO_4$ tetragonal regions with promising *Qf*. Solid solutions are one of the most important methods to design temperature stable microwave dielectric ceramics using two end members with opposite TCF. However, even though the two end members possess

View Article Online
DOI: 10.1039/C8TC02260G

–ve TCF, a series temperature stable microwave dielectric ceramics can be achieved, e.g. $BiVO_4$-$CaMoO_4$, $BiVO_4$-$CaWO_4$, $BiVO_4$-$(Na_{0.5}Ln_{0.5})MoO_4$ due to the large +ve TCF in the Bi-rich tetragonal scheelite phase, which is similar to trends within the $BiVO_4$-$LnVO_4$ system, as discussed in chapter 3.1.1.

3.3.3 ($A^{3+}B^{5+}$) (A = Ln, Y , Sc etc.; B = Nb, Ta, Sb, P and $(Ti_{1/2}W_{1/2})^{5+}$) complex substitutions

Although these complex systems have the same valence on both A and B site as $BiVO_4$, only limited efforts have been made to study their influence on the structure and properties. The most studied are isovalent dopants based on the rare-earth orthoniobates, $LnNbO_4$. This class of oxides undergoes a reversible ferroelastic phase transition from the fergusonite structure (monoclinic, C2/c) to a tetragonal scheelite structure (tetragonal, $I4_1/a$) at high temperature between 480 ~ 860^oC depending on ionic radius,[141-144] which is similar to that of monoclinic $BiVO_4$. In addition, similar motion and annihilation of ferroelastic domains with pressure and temperature have been observed in $BiVO_4$ and $LnNbO_4$.[145] However, Raman scattering has shown that the phase transition in $BiVO_4$ is related to an optic soft mode where as in $LaNbO_4$ its origin differs.[146] In 2017, we studied the phase evolution and microwave dielectric properties of $(1-x)BiVO_4$–$xLaNbO_4$ ($0.0 \le x \le 1.0$) ceramics.[147] A monoclinic scheelite solid solution was obtained for $0 \le x \le 0.08$ and a tetragonal solid solution was obtained for $0.08 < x < 0.7$, as shown in Fig. 27. At $x > 0.7$, tetragonal scheelite, monoclinic $LaNbO_4$-type and $La_{1/3}NbO_3$ phases co-existed. A significant difference from the discussion presented in Chapter 3.3.2 is that in the monoclinic solid solution, high temperature accelerates the formation of the tetragonal phase, Fig. 28. The characteristic peaks of (200) and (020) remained split for x = 0.08 sintered at 680 ^oC

View Article Online
DOI: 10.1039/C8TC02260G

but merged into a single peak at a higher sintering temperature ~ 710 ^{o}C. The changes in the structure as a function of sintering temperature most likely relate to the rate diffusion and / or solid solubility of Nb in the V tetrahedral network. It also worth noting that Nb substitution for V improved the temperature stability of *Qf* over a wide range, 20 ~ 140 ^{o}C. The slight change in the value of x for the monoclinic/tetragonal phase boundary (x = 0.08 in case of $LaNbO_4$) compared with Mo substitution on B site (x = 0.1) is attributed to the larger ionic radius of Nb^{5+} with respect to Mo^{6+}. To date, this is the only case, in which a ferroelastic fergusonite phase was used to form a solid solution with $BiVO_4$ but other rare earth niobates such as $NdNbO_4$ and $SmNbO_4$, are expected to have a similar effect on structure and properties. The complex substitution of both A^{3+} and B^{5+} for Bi^{3+} and V^{5+} in $BiVO_4$ needs to be studied further but the preliminary results discussed above on simple A^{3+} and B^{5+} substitutions point towards potential key aspects for design strategies for complex substitution.

Another group of tetragonal scheelite $Re(Ti_{0.5}W_{0.5})O_4$ (Re = Pr, Nd, Sm, Gd, Tb, Dy, and Y) was reported by Sebastian et al. in 2003.[148] Usually Ti prefers to be 6 coordinated in complex oxides and it is rare it that occupies the B site in the BO_4 tetrahedra in the scheelite structure. Moreover, $Re(Ti_{0.5}W_{0.5})O_4$ ceramics have ε_r = 20 with *Qf* > 6,000 GHz and this might be useful substituents into $BiVO_4$.

3.3.4 ($A^{4+}B^{4+}$) (A = Zr, Hf, U; B = Ge) complex substitutions

$ZrGeO_4$ is the first reported $A^{4+}B^{4+}O_4$ type scheelite material.[149] It may be synthesized via solid state reaction but soft chemical methods lead to the formation of zircon type $ZrGeO_4$, which transforms to scheelite above 1180 ^{o}C.[150-152] In Cheng el al.'s work,[153] two high-pressure phases of $ZrGeO_4$, fergusonite (isomorphic to $LnNbO_4$) and an un-known monoclinic structure were reported, the schematic of

View Article Online
DOI: 10.1039/C8TC02260G

phase transitions between these four polymorphs is given in Fig. 29. $HfGeO_4$, $ThGeO_4$ and $GeUO_4$ were also reported to possess a tetragonal scheelite structure.[154,155] Given the same crystal structure and similar cell parameters with that of $BiVO_4$, the $(1-x)BiVO_4$-$xA^{4+}B^{4+}O_4$ system might have potential for interesting structure-property relations within the solid solution but to date, there have been no reports on these compositions.

3.4 A site defect type ($\Phi_{1/3}A^{3+}_{2/3}B^{6+}O_4$)

The only defects that occur in large concentrations in the scheelite structure are A cation vacancies. Such defect phases are represented as $A_{1-x}\Phi_xMO_4$ where Φ is a vacancy on the A site. The maximum value of x = 1/3 with the scheelite structure was found for $La_{2/3}\Phi_{1/3}MoO_4$. If quenched from high temperature[156,157] vacancies are randomly distributed but if cooled slowly, become ordered in a similar manner to $Ln_{2/3}MoO_4$ and $Bi_{2/3}MoO_4$.[158-160] As summarized by Sleight and Linn,[161] there are three different types of order reported as shown in Fig. 30, which give rise to unique distortions of the MoO_4 tetrahedra. Since quenching suppresses tetrahedral distortion, the formation of a solid solution with a stable scheelite structure may also give rise to the same phenomenon. $A_{2/3}\Phi_{1/3}MoO_4$ has been shown to form a scheelite solid solution with $BiVO_4$ but only within a limited range.[162] In addition, defect concentrations may also be modified by forming solid solutions of $A_{2/3}\Phi_{1/3}MoO_4$ with $(A^{+}_{0.5}Ln_{0.5})MoO_4$ or $A^{2+}MoO_4$ systems.

In previous work,[163] the full compositional range of $xBi_{2/3}MoO_4$–$(1-x)BiVO_4$ ($0.0 \leq x \leq 1.0$) was prepared via the solid state reaction method. The phase diagram is separated into at least four regions as shown in Fig. 31: I, scheelite monoclinic phase region with $0.0 \leq x \leq 0.1$; II, scheelite tetragonal phase region with $0.1 < x < 0.5$; III,

View Article Online
DOI: 10.1039/C8TC02260G

an ordered scheelite phase region with $0.5 \leq x < 0.7$ and IV, a composite phase region with $0.7 \leq x < 1.0$ (ordered scheelite and monoclinic $Bi_{2/3}MoO_4$ phase). ε_r of the $xBi_{2/3}MoO_4$–$(1-x)BiVO_4$ ceramics reaches a maximum of ~ 75, lower than that in non-defective $BiVO_4$-$(A_{0.5}Bi_{0.5})MoO_4$ type, at x = 0.1 with *Qf* ~ 8,000 GHz. However, ε_r decreased with further increase of $Bi_{2/3}MoO_4$ concentration and *Qf* deteriorated in mixed phase regions.

A series of the $(1-x)BiVO_4$-$xLa_{2/3}MoO_4$ ceramics were prepared via solid solution reaction method in our previous work.[164] As shown in Fig. 32, as x increased from 0 to 0.1, the crystal structure changed continuously from a monoclinic to a tetragonal scheelite structure. When x increased to 0.9, co-existence of tetragonal scheelite and $La_{2/3}MoO_4$ phases was observed. All ceramics densified below 800 °C. $68 \geq \varepsilon_r \geq 73$ was achieved in compositions with $x \leq 0.10$ with *Qf*~10,000 GHz. However, the phase transition between monoclinic and tetragonal scheelite structures resulted in large negative/positive TCF. Similar results were also obtained in other $BiVO_4$-$Ln_{2/3}MoO_4$ ceramics[165] and it seems that A site defects decrease ε_r without improving *Qf*.

3.5 Composite ceramics

TCF is an important physical parameter for microwave dielectric ceramics. Most microwave dielectric ceramics with low ε_r (below 20) possess -ve TCF while most high ε_r (> 40) possess +ve TCF.[26,30,31] Rutile TiO_2, perovskite $CaTiO_3$ and $SrTiO_3$ are three archetype ceramics with high ε_r, high *Qf* values and large positive TCF values.[166-169] However, high ε_r microwave dielectric ceramics with large negative TCF are rare and all -ve TCF materials with − 200 ppm/°C are also listed in Table 2.[170-173]

View Article Online
DOI: 10.1039/C8TC02260G

Among them, $BiVO_4$ is attractive due to its high *Qf* and low sintering temperature. In applications, near zero TCF is required to keep the electronic devices work normally in a wide environmental temperature range (− 25 °C ~ + 85 °C). Usually there are two effective methods to modify the TCF: i) solid solution or ii) composite ceramics. Solid solutions have been discussed in detail in previous sections and in this chapter, composites with $BiVO_4$ are discussed.

$BiVO_4$-TiO_2 system

According to Lv's report on Bi_2O_3-TiO_2-V_2O_5 ternary diagram,[174,175] three single phase compounds, $Bi_{17}V_2TiO_{32.5}$, $Bi_4V_{1.5}Ti_{0.5}O_{10.85}$ and $Bi_{13}V_5TiO_{34}$ exist in the Bi_2O_3–TiO_2–V_2O_5 ternary system but no single-phase compounds are reported in the V_2O_5-TiO_2 and TiO_2-$BiVO_4$ binary systems, Fig. 33. This indicates that TiO_2 and $BiVO_4$ phases do not react with each other and could co-exist. Furthermore, the absence of single phase compounds in the TiO_2-$BiVO_4$ binary system suggests that immiscible composites may be fabricated. TiO_2 has been reported to have $\varepsilon_r = 100$ and $Qf \sim 14{,}000$ GHz but TCF > + 400 ppm/°C.[166] In previous work,[176] the chemical compatibility between $BiVO_4$ and TiO_2 was confirmed by XRD and EDS analysis, Fig. 34. Almost all the (1-x)$BiVO_4$-xTiO_2 (x = 0.4, 0.50, 0.55 and 0.60) densify at ≤ 900 °C. If the sintering temperature is increased, composite samples melt. ε_r increased linearly from 68.5 at x = 0.0 to 87.7 at x = 0.6, accompanied by a commensurate increase in TCF from – 260 ppm/°C for pure $BiVO_4$ to + 46 ppm/°C at x = 0.6. Near-zero TCF (– 8 ppm/°C) was achieved in compositions with x = 0.55. However, *Qf* did not increase linearly with the concentration of TiO_2. First, *Qf* increased to ~12,290 GHz at x = 0.4 but then decreased to 9,500 GHz at x = 0.55. Therefore, a series of modified rutile structured $Ti_{1-x}(Cu_{1/4}Nb_{3/4})_xO_2$ ($\varepsilon_r \sim 95$, $Qf \sim 35{,}000$ GHz, TCF ~ + 400 ppm/°C)[177] with low sintering temperatures were chosen to replace pure

View Article Online
DOI: 10.1039/C8TC02260G

TiO_2 with $Bi(Fe,Mo,V)O_4$ and $(Na,Bi)(Mo,V)O_4$ series[55,56] replacing $BiVO_4$. In addition, nano-sized TiO_2 (20 nm) particles were also utilized. However, none of these modifications increased Qf which remained between 9,000 ~ 12,330 GHz, possibly due to the difference in the sintering temperature of the end members. Nonetheless, excellent microwave dielectric properties with a $\varepsilon_r \sim 86$, $Qf \sim 9{,}500$ GHz and near-zero TCF ~ − 8 ppm/°C were obtained in the $0.45BiVO_4$-$0.55TiO_2$ ceramics sintered 2 h at 900 °C.

$BiVO_4$-TiO_2-$Bi_2Ti_4O_{11}$ system

In the Bi_2O_3-TiO_2 binary system, $Bi_2Ti_4O_{11}$ is the last binary single compound in TiO_2-rich region and co-fires with TiO_2. Undoped $Bi_2Ti_4O_{11}$ ceramic was reported to possess a $\varepsilon_r = 53.2$, $Qf \sim 4{,}500$ GHz (at 5 GHz), and TCF = − 550 ppm/°C.[170] Hence, temperature stable microwave dielectric ceramics, $0.919TiO_2$-$0.081Bi_2O_3$, composed of TiO_2 and $Bi_2Ti_4O_{11}$, possess high $\varepsilon_r \sim 80$, high Q (1800 at 5 GHz) and TCF ~ +21 ppm/°C.[178] Therefore, based on the discussion above, a series of temperature stable microwave dielectric ceramics might be achievable in the $BiVO_4$-TiO_2-$Bi_2Ti_4O_{11}$ ternary system along the tie line, $(0.88TiO_2$-$0.12Bi_2Ti_4O_{11})$-$(0.45BiVO_4$-$0.55TiO_2)$ shown in Fig. 33. Improvements in processing this system might also increase *Qf*.

$BiVO_4$-$CaTiO_3$ and $BiVO_4$-$SrTiO_3$ system

According to simple mixing rules, either 24.5 mol. % $CaTiO_3$ or 17.8 mol. % $SrTiO_3$ in a composite with $BiVO_4$ shifts TCF to near zero. However, according to our unpublished data on these two system, secondary phases containing Bi, (Ca,Sr) and Ti, probably the Aurivillius phases, $SrBi_4Ti_4O_{15}$ and $CaBi_4Ti_4O_{15}$, were detected in the ceramics, leading to poor *Qf*.

View Article Online
DOI: 10.1039/C8TC02260G

4. Summary and future work

Some key conclusions can be drawn from the work presented in this review:

1. Monoclinic $BiVO_4$ has an unusual scheelite structure which transforms to standard tetragonal scheelite structure at 255 ^oC, under external pressure (16 kbar) or through equivalent internal pressure caused by B-site substitution. The solid solubility of monoclinic $BiVO_4$ can be extended to 10 mol.% by the stoichiometric substitution of (A^+Ln^{3+}) and Mo^{6+} on the A and B site, resulting in a transition to a tetragonal phase. Only La or Ce of the Ln ions can occupy the Bi^{3+}site of monoclinic $BiVO_4$, confirmed by the shift in the phase transition temperature recorded through anomalies in thermal expansion. However, there is no evidence that a single substitution on the A site results in a phase transition to a tetragonal phase. All monoclinic $BiVO_4$ solid solutions irrespective of the A/B site substituents possess a lower phase transition temperature than that of pure $BiVO_4$ (255 ^oC).

2. Some techniques are ideal at determining the phase transition in monoclinic $BiVO_4$ solid solutions. With *in-situ* XRD, merging of characteristic XRD peaks, to attain equal *a* and *b* cell parameters, accompanied by transformation of the gamma angle to 90^o are key metrics that define the onset of the phase transition. Similarly, merging of some characteristic vibration modes at the phase transition, caused by the relaxation of distorted BO_4 tetrahedra to give two equal BO bond lengths can be observed using *in-situ* Raman and infrared spectra. Sudden changes in the thermal expansion coefficient (monoclinic and tetragonal scheelite are about + 5 ppm/^{o}C and + 14 ppm/^{o}C, respectively) can also be used to determine the phase transition temperature. Finally, according to LST relation, a peak value of ε_r will occur at the phase transition temperature.

View Article Online
DOI: 10.1039/C8TC02260G

3. The presence of a peak value of ε_r in the $BiVO_4$ solid solution ceramics at the phase transition allows substitutions, such as $(ALn^{3+})MoO_4$ to optimize properties (ε_r increases from 68 to 81) by lowering the transformation to room temperature. The peak in ε_r occurs in $BiVO_4$-$(Li_{0.5}Bi_{0.5})MoO_4$ ceramics for example, because a minimum value of cell volume is achieved at the phase boundary. ε_r is determined by cell volume and molecular polarizability, hence if the polarizability of substitution ions is smaller than that of Bi^{3+}, ε_r might decrease linearly with decreasing Bi content. *Qf* often reach a maximum value in phase boundary compositions because the atomic packing factor is optimized. The highest *Qf* (~ 13,000 GHz) was obtained in $0.02Bi(Fe_{1/3}Mo_{2/3})O_4$–$0.98BiVO_4$ ceramics sintered at 820 ^oC with a $\varepsilon_r \sim 74.8$. Due to the existence of phase transition, however, temperature stable ceramic cannot be achieved in solid solutions. Phase transition temperatures above 85 ^oC lead to a large –ve TCF (− 200 ppm/^oC, monoclinic) but below room temperature a large +ve TCF (+ 200 ppm/^oC, tetragonal) between 25 ~ 85 ^oC. However, layered or granulated particles composites containing two compositions with negative and positive TCF values, respectively, may achieve temperature stable composite ceramics with high permittivity. Compatible compositions with large +ve TCF end members such as TiO_2 (TCF = + 400 ppm/^oC) permit the design of composite ceramics with $BiVO_4$. A range of temperature stable microwave dielectric ceramics suitable for LTCC applications are also predicted in the $BiVO_4$-TiO_2-$Bi_2Ti_4O_{11}$ system.

4. To date, all the studies on the modification of $BiVO_4$ ceramics have been limited to $BiVO_4$-ABO_4 binary systems. Since scheelite is an adaptable structure-type, novel microwave dielectric properties might be achieved in ternary or quaternary systems. Since both V_2O_5 and MoO_3 powders are partially water soluble, the $BiVO_4$-$(A^+Bi)MoO_4$ materials might be suitable for cold sintering.[181] Cold-sintered

View Article Online
DOI: 10.1039/C8TC02260G

temperature stable $Na_{0.5}Bi_{0.5}MoO_4$-Li_2MoO_4 composite ceramics have already been reported[182] and thus $BiVO_4$ based materials might be promising candidates for fabrication using sustainable and green synthesis methods.

5. Acknowledgements

This work was supported by Sustainability and Substitution of Functional Materials and Devices EPSRC (EP/L017563/1), the National Key Research and Development Program of China (2017YFB0406301), the National Natural Science Foundation of China (U1632146), the Young Star Project of Science and Technology of Shaanxi Province (2016KJXX-34), the Key Basic Research Program of Shaanxi Province (2017GY-129), the Fundamental Research Funds for the Central University, and the 111 Project of China (B14040).

View Article Online
DOI: 10.1039/C8TC02260G

6. References

1. W. F. DeJong, J. J. Delange, *Am. Mineral.* 1936, **21**, 809.
2. M. M. Qurashi, W. H. Barnes, *Am. Mineral.* 1952, **37**, 423.
3. M. M. Qurashi, W. H. Barnes, *Am. Mineral.* 1953, **38**, 489.
4. R. S. Roth, J. L. Waring, *Am. Mineral.* 1963. **48**, 1348.
5. H. E. Swanson, M. C. Morris, J. H. deGroot, E. H. Evans, *NBS Report*, 1962, **7592**, 2.
6. E. F. Dudnik, V. V. Gene, S. V. Akimov, A. Ya. Kreicherek, *Soviet Physics, Solid state*, 1974, **16**, 2733.
7. J. D. Bierlein, A. W. Sleight, *Solid State Commu.* 1975, **16**, 69.
8. W. I. F. David, A. M. Glazer, A. W. Hewat, *Phase Transit.* 1979, **1**, 155.
9. A. W. Sleight, H. Y. Chen, A. Ferretti, D. E. Cox, *Mater. Res. Bull.* 1980, **14**, 1571.
10. A. Pinczuk, G. Brown, F. H. Dacol, *Solid State Commun.* 1977, **24**, 163.
11. A. Pinczuk, B. Welber, F. H. Dacol, *Solid State Commun.* 1979, **29**, 515.
12. C. Manolikas, S. Amelinckx, *Phys. Status Solidi* 1980, **60**, 167.
13. I. G. Wood, B. Welber, W. I. F. David, A. M. Glazer, *J. Appl. Crystallogr.* 1980, **13**, 224.
14. G. Benyuan, M. Copic, H. Z. Cummins, *Phys.Rev. B* 1981, **24**, 7.
15. A. Kudo, K. Omori, H. Kato, *J. Am. Chem. Soc.* 1999, **121**, 11459.
16. H. Wienand, W. Ostertag, K. Bittler, 1984, US Patent 4455174.
17. J. F. Higgins, 1977, U.S. Patent 4063956.
18. R. G. Li, F. X. Zhang, D. G. Wang, J. X. Yang, M. R. Li, J. Zhu, X. Zhou, H. X. Han, C. Li, *Nat. Commun.* 2013, **4**, 1432.

View Article Online
DOI: 10.1039/C8TC02260G

19. H. Ye, J. Lee, J. S. Jang, A. J. Bard, *J. Phys. Chem. C* 2010, **114**, 13322.

20. S. Kohtani, M. Tomohiro, K. Tokumura, R. Nakagaki, *Appl. Catal. B-Environ.* 2005, **58**, 265

21. C. Li, P. Zhang, R. Lv, J. Lu, T. Wang, S. Wang, H. Wang, J. Gong, *Small*, 2013, **9**, 3951.

22. R.W. Hess, 1978, G.B. Patent 1585524.

23. P. Koehler, P. Ringe, H. Heine, 1984, Patent DE 334850.

24. R. M. Sullivan, 1991, EP Patent 443981.

25. R. D. Richtmyer, *J. Appl. Phys.* 1939, **10**, 391.

26. I. M. Reaney, D. Iddles, *J. Am. Ceram. Soc.* 2006, **89**, 2063.

27. D. Zhou, L. X. Pang, D. W. Wang, C. Li, B. B. Jin, I. M. Reaney, *J. Mater. Chem. C* 2017, **5**, 10094.

28. M. Valant, D. Suvorov, *J. Am. Ceram. Soc.* 2000, **83**, 2721.

29. S. H. Wee, D. W. Kim, S. I. Yoo, *J. Am. Ceram. Soc.* 2004, **87**, 871.

30. M. T. Sebastian, R. Ubic, H. Jantunen, *Int. Mater. Rev.* 2015, **60**, 392.

31. M. T. Sebastian, H. Jantunen, *Int. Mater. Rev.* 2008, **53**, 57.

32. D. Zhou, C. A. Randall, H. Wang, L. X. Pang, X. Yao, *J. Am. Ceram. Soc.* 2010, **93**, 2147.

33. K. Momma, F. Izumi, *J. Appl. Crystallogr.* 2011, **44**, 1272.

34. https://zh.mindat.org.

35. J. Granzin, D. Pohl, *Z. Kristallogr.* 1984, **169**, 289.

36. O. V. Knorring, Th. G. Sahama, M. Lehtinen, P. Rehtijärvi, J. Siivola, *Contr. Mineral. Petrol.*1973, **41**, 325.

37. K. Mereiter, A. Preisinger, *Mathematich-NaturwissenschaftlicheKlasse, Sitzungsberichte*, 1986, **123**, 79.

View Article Online
DOI: 10.1039/C8TC02260G

38.G. Dreyer, E. Tillmanns, *NeuesJahrbuchfuerMineralogie. Monatshefte (Band=Jahr)*, 1981, 151.

39. H. Fan, T. Jiang, H. Li, D. Wang, L. Wang, J. Zhai, D. He, P. Wang, T. Xie, *J. Phys. Chem. C* 2012, **116**, 2425.

40. X. Zhang, Z. H. Ai, F. L. Jia, L. Z. Zhang, X. X. Fan, Z. G. Zou, *Mater. Chem. Phys.* 2007, **103**, 162.

41. C. G. Li, G. S. Pang, S. M. Sun, S. H. Feng, *J. Nanopart. Res.* 2010, **12**, 3069.

42. Nat. Bur. STDS. (U. S.) Mono. 1964, **25**, Sec. 3, 14-15

43. A. K. Bhattacharya, K. K. Mallick, A. Hartridge, *Mater. Lett.* 1997, **30**, 7.

44. P. J. Bridge, M. W. Pryce, *Mineral. Mag.*1974, **39**, 847.

45. A. W. Sleight, H. Chen, A. Ferretti, D. E.Cox, *Mater. Res. Bull.* 1979, **14**, 1571.

46. R. M. Hazen, J. W. E. Mariathasan, *Science* 1982, **216**, 991.

47. J. W. Anthony, R. A. Bideaux, K. W. Bladh, M. C. Nichols, *Handbook of Mineralogy Volume IV arsenates, phosphates and vanadates.*; Mineral Data Publishing, Tuscon, Arizona, 2000, USA, Vol. IV.

48. E. S. Fisher, *J. Phys.: Condens. Matter* 1989, **1**, 2875.

49. K. Hirota, G. Komatsu, M. Yamashita, H. Takemura, O. Yamaguchi, *Mater. Res. Bull.* 1992, **27**, 823.

50. J. W. E. Mariathasan, R. M. Hazen, L. W. Finger, *Phase Trans.*1986, **6**,165.

51. S. Tokunaga, H. Kato, A. Kudo, *Chem. Mater.* 2001, **13**, 4624.

52. J. Granzin, D. Pohl, *Z. Kristallogr.* 1984, **169**, 289.

53. M. W. Stoltzfus, P. M. Woodward, R. Seshadri, J. H. Klepeis, B. Bursten, *Inorg. Chem.* 2007, **46**, 3839.

54. L. S. Wainer, R. F. Baggio, H. L. Dussel, M. A. R. Benyacar, *Ferroelectrics* 1981, **31**, 121.

View Article Online
DOI: 10.1039/C8TC02260G

55. D. Zhou, L. X. Pang, H. Wang, J. Guo, X. Yao, C. A. Randall, *J. Mater. Chem.* 2011, **21**, 18412.

56. D. Zhou, L. X. Pang, J. Guo, Z. M. Qi, T. Shao, X. Yao, C. A. Randall, *J. Mater. Chem.* 2012, **22**, 21412.

57. D. Zhou, L. X. Pang, J. Guo, H. Wang, X. Yao, C. A. Randall, *Inor. Chem.* 2011, **50**, 12733.

58. Ferro, http://www.ferro.com/.

59. Dupont, http://www.dupont.com/.

60. X. M. Chen, Y. Li, *J. Am. Ceram. Soc.* 2002, **85**, 579.

61. Y. Ota, K. Kakimoto, H. Ohsato, *J. Eur. Ceram. Soc.* 2004, **24**, 1755.

62. H. Takahashi, Y. Baba, K. Ezaki, *Jpn. J. Appl. Phys.* 1996, **35**, 5069.

63. J. Kato, H. Kagata, K. Nishimoto, *Jpn. J. Appl. Phys.* 1992, **31**, 3144.

64. D. Zhou, L. X. Pang, Z. M. Qi, *Inor. Chem.* 2014, **53**, 9222.

65. L. X. Pang, D. Zhou, Z. M. Qi, W. G. Liu, Z. X. Yue, I. M. Reaney, *J. Mater. Chem. C*, 2017, **5**, 2695.

66. R. D. Shannon, *Acta Crystallogr., Sect. A: Cryst. Phys., Diffr., Theor. Gen. Crystallogr.* 1976, **A32**, 751.

67. D. Errandonea, C. Popescu, S. N. Achary, A. K. Tyagi, M. Bettinelli, *Mater. Res.Bull.*2014, **50**, 279.

68. D. Errandonea, J. Pellicer-Porres, D. Martinez-Garcia, J. Ruiz-Fuertes, A. Friedrich, W. Morgenroth, C. Popescu, P. Rodriguez-Hernandez, A. Munoz, M. Bettinelli, *J. Phys. Chem. C* 2016, **120**, 13749.

69. Y. Oka, T. Yao, N. Yamamoto, *J. Solid State Chem.* 2000, **152**, 486.

70. M. R. Dolgos, A. M. Paraskos, M. W. Stoltzfus, S. C. Yarnell, P. M. Woodward, *J. Solid State Chem.* 2009, **182**, 1964.

View Article Online
DOI: 10.1039/C8TC02260G

71. H. Xu, C. Wu, H. Li, J. Chu, G. Sun, Y. Xu, Y. Yan, *Appl. Surf. Sci.* 2009, **256**, 597.

72. P. Kwolek, K. Pilarczyk, T. Tokarski, K. Lewandowska, K. Szaciłowski, *Nanoscale* 2014, **6**, 2244.

73. M. Dragomir, I. Arcon, S. Gardonio, M. Valant, *Acta Mater.* 2013, **61**, 1126.

74. D. Zhou, L. X. Pang, J. Guo, Z. M. Qi, T. Shao, Q. P. Wang, H. D. Xie, X. Yao, C. A. Randall, *Inor. Chem.* 2014, **53**, 1048.

75. Y. Wang, R. Zuo, C. Zhang, J. Zhang, T. Zhang, *J. Am. Ceram. Soc.*2015, **98**, 1.

76. M. C. Neves, M. Lehocky, R. Soares, Jr. L. Lapcik, T. Trinidade, *Dyes. Pigm.* 2003, **59**, 181.

77. H. Xu, C. Wu, H. Li, J. Chu, G. Sun, Y. Xu, *Appl. Surf. Sci.* 2009, **256**, 597.

78. Q. Wang, N. An, R. Mu, H. Liu, J. Yuan, J. Shi, W. Shangguan, *J. Alloys Compd.* 2012, **522**, 19.

79. D. Zhou, W. B. Li, H. H. Xi, L. X. Pang, G. S. Pang, *J. Mater. Chem. C* 2015, **3**, 2582.

80. D. Zhou, J. Li, L. Pang, G. Chen, Z. Qi, D. Wang, I. M. Reaney, *ACS Omega* 2016, **1**, 963.

81. A. Zhang, J. Zhang, *J. Hazard Mater.* 2010, **173**, 265.

82. A. Zhang, J. Zhang, *Chin. J. Chem. Phys.* 2010, **23**, 73.

83. W. Zhao, Y. Wang. Y. Yang, J. Tang, Y. Yang, *Appl. Catal. B* 2012, **115-116**, 90.

84. M. Agunaou, B. Mernari, J. M. Tatibouët, *Appl. Catal. A* 2000, **196**, 87.

85. T. H. Yeom, S. H. Choh, C. Rudowicz, M. S. Jang, *Appl. Magn. Reson.*1999, **16**, 23.

86. J. Z. Yin, S. B. Huang, Z. C. Jian, M. L. Pan, Y. Q. Zhang, Z. B. Fei, X. R. Xu, *Appl. Phys. A* 2015, **120**, 1529.

View Article Online
DOI: 10.1039/C8TC02260G

87. D. Zhou, B. He, J. Guo, L. X. Pang, Z. M. Qi, T. Shao, Q. P. Wang, Z. X. Yue, X. Yao, *J. Am. Ceram. Soc.* 2014, **97**, 2915.

88. B. Robertson, E. Kostiner, *J. Solid State Chem.* 1972, **4**, 29.

89. R. S. Roth, J. L. Waring, *J. Res. National Bur. Standards Sec. A-Phys. Chem.* 1962, **66**, 451.

90. C. Lee, R. Marquart, Q. Zhou; B. J. Kennedy, *J. Solid State Chem.* 2003, **174**,310.

91. O. Monfort, S. Sfaelou, L. Satrapinskyy, T. Plecenik, T. Roch, G. Plesch, P. Lianos, *Catal. Today* 2017, **280**, 51.

92. Z. Zhao, W. Luo, Z. Li, Z. Zou, *Phys. Lett. A* 2010, **374**, 4919.

93. L. S. Kumari, P. P. Rao, A. N. P. Radhakrishnan, V. James, S. Sameera, P. Koshy, *Solar Energy Mater. Solar Cells* 2013, **112**, 134.

94. A. Loiudice, J. Ma, W. S. Drisdell, T. M. Mattox, J. K. Cooper , T. Thao, C. Giannini, J. Yano, L. Wang, I. D. Sharp, R. Buonsanti, *Adv. Mater.* 2015, **27**, 6733.

95. A. W. Sleight, W. Jeitschko, *Mater. Res. Bull.*1974, **9**, 951.

96. W. Jeitschko, A. W. Sleight, W. R. McClellan, J. F. Weiher, *Acta Crystallogr. B* 1976, **32**, 1163.

97. M. V. Mokhosoev, E. G. Khaikina, L. M. Kovba, Z. G. Bazarova, N. L. Kishkin, S. D. Tudupova, *ZhurnalNeorganicheskoiKhimii* 1987, **32**, 1713.

98. U. Kolitsch, E. Tillmanns, *Acta Crystallogr. Sec. E* 2003, **59**, I43.

99. C. Palache, H. Berman, C. Frondel, 1951, Dana's system of mineralogy, (7th edition), v. II, 1075–1077.

100. R. M. Hazen, L.W. Finger, J. W. E. Mariathasan, *J. Phys. Chem. Solids* 1985, **46**, 253.

101. G. K. Choi, J. R. Kim, S. H. Yoon, *J. Eur. Ceram. Soc.* 2007, **27**, 3063.

102. S. H. Yoon, D. W. Kim, S. Y. Cho, *J. Eur. Ceram. Soc.* 2006, **26**, 2051.

View Article Online
DOI: 10.1039/C8TC02260G

103. E. S. Kim, B. S. Chun, R. Freer, R. J. Cernik, *J. Eur. Ceram. Soc.* 2010, **30**, 1731.

104. W. Yao, J, Ye, J. *Phys. Chem. B* 2006, **110**, 11188.

105. S. Sameera, P. P. Rao, S. Divya, A. K. V. Raj, T. R. Ajuthara, *Energ. Buildings* 2017, **154**, 491.

106. W. Yao, J. Ye, *Catal. Today* 2006, **116**, 18.

107. S. F. Sameera, P. P. Rao, L. S. Kumari, P. Koshy, *Chem. Lett.* 2009, **38**, 1088.

108. Y. Ding, J. Bian, *Ceram. Int.* 2013, **39**, 1555.

109. M. V. Saveleva, I. V. Shakhno, V. E. Plyushchev, *Inor. Mater.* 1970, **6**, 1466.

110. P. V. Lvevtsov, L. P. Kozeeva, *Inor. Mater.* 1969, **5**, 1571.

111. L. X. Pang, D. Zhou, J. Guo, Z. X. Yue, X. Yao, *J. Am. Ceram. Soc.* 2015, **98**, 130.

112. D. Zhou, C. A. Randall, L. X. Pang, H. Wang, J. Guo, G. Q. Zhang, Y. Wu, K. T. Guo, L. Shui, X. Yao, *Mater. Chem. Phys.* 2011, **129**, 688.

113. H. H. Xi, D. Zhou, H. H. Xie, W. B. Li, *Mater. Lett.* 2015, **142**, 221.

114. H. H. Xi, D. Zhou, H. H. Xie, B. He, Q. P. Wang, *J. Am. Ceram. Soc.* 2015, **98**, 587.

115. H. H. Xi, D. Zhou, H. H. Xie, W. B. Li, *Ceram. Int.* 2015, **41**, 6103.

116. D. Zhou, L. X. Pang, J. Guo, *Funct. Mater. Lett.* 2012, **5**, 1250042.

117. L. X. Pang, D. Zhou, Z. Qi, Z. Yue, *Sci. Rep.* 2017, **7**, 3201.

118. D. Zhou, L. X. Pang, H. D. Xie, J. Guo, B. He, Z. M. Qi, T. Shao, X. Yao, C. A. Randall, *Eur. J. Inor. Chem.* 2014, **2**, 296.

119. J. S. Kim, J. C. Lee, C. I. Cheon, H. J. Kang, *Jpn. J. Appl. Phys.* 2006, **45**, 7397.

120.H. Yang, Y. Lin, J. Zhu, F. Wang, Z. Dai, *J. Alloys Compd.* 2010, **502**, L20.

121. H. Zhou, H. Wang, K. Li, M. Zhang, H. Yang, *J. Mater. Sci.: Mater. in*

View Article Online
DOI: 10.1039/C8TC02260G

*Electron.*2010, **21**, 252.

122. D. Zhou, W. B. Li, J. Guo, L. X. Pang, Z. M. Qi, T. Shao, H. D. Xie, Z. X. Yue, X. Yao, *Inor. Chem.* 2014, **53**, 5712.

123. D. Zhou, C. Randall, H. Wang, L. X. Pang, X. Yao, *J. Am. Ceram. Soc.* 2010, **93**, 1096.

124. D. Zhou, W. G. Qu, C. A. Randall, L. X. Pang, H. Wang, X. G. Wu, J. Guo, G. Q. Zhang, L. Shui, Q. P. Wang, H. C. Liu, X. Yao, *Acta Mater.* 2011, **59**, 1502.

125. R. H. Lyddane, H. Sachs, E. Tellar, *Phys. Rev.* 1941, **59**, 673.

126. D. Zhou, L. X. Pang, W. G. Qu, *RSC Adv.* 2013, **3**, 5009.

127. P. V. Klevtsov, V. A. Vinokurov, R. F. Klevtsova, *Sov. Phys. Crystallogr.* 1974, **18**, 749.

128. P. V. Klevtsov, V. A. Vinokurov, *Sov. Phys. Crystallogr.*1975, **19**, 474.

129. R. F. Klevtsova, *Kristallogr.* 1975, **20**, 746.

130. S. Sameera, P. P. Rao, V. James, S. Divya, A. K.V. Raj, *Dyes Pigments* 2014, **104**, 41.

131. S. Sameera, P. P. Rao, S. Divya, A. K. V. Raj, *ACS Sus. Chem. Eng.* 2015, **3**, 1227.

132. P. V. Klevtsov, V. I. Protasova, L. Y. Kharchenko, R. F. Klevtsova, *Sov. Phys. Crystallogr. (Engl. Transl.)*1974, **18**, 523.

133. R. F. Klevtsova, *Sov. Phys. Crystallogr. (Engl. Transl.)* 1975, **20**, 456.

134. J. M. Postema, W. T. Fu, D. J. W. Ijdo, *J. Solid State Chem.* 2011, **184**, 2004.

135. X. Huang, Z. Lin, L. Zhang, J. Chen, G. Wang, *Crys. Growth Design* 2006, **6**, 2271.

136. G. H. Chen, F. F. Gu, M. Pan, L. Q. Yao, M. Li, X. Chen, Y. Yang, T. Yang, C. L. Yuan, C. R. Zhou, *J. Mater. Sci.: Mater. Electro.*2015, **26**, 6511.

View Article Online
DOI: 10.1039/C8TC02260G

137. F. Gu, G. Chen, X. Kang, X. Li, C. Zhou, C. Yuan, Y. Yang, T. Yang, *J. Mater. Sci.* 2015, **50**, 1295.

138. D. Zhou, L. X. Pang, Z. M. Qi, X. Yao, *Inor. Chem.* 2014, **53**, 9222.

139. V. Nassif, R. E. Carbonio, J. A. Alonso, *J. Solid State Chem.* 1999, **146**, 266.

140. R. D. Shannon, *J. Appl. Phys.* 1993, **73**, 348.

141. K. A. Gingerich, H. E. Bair, *Adv. X-Ray Anal.* 1964, **7**, 22.

142. D. Kim, D. Kwon, S. Yoon, K. Hong, *J. Am. Ceram. Soc.* 2006,**89**, 3861.

143. P. Sarin, R. W. Hughes, D. R. Lowry, Z. D. Apostolov, W. M. Kriven, *J. Am. Ceram. Soc.* 2014,**97**, 3307.

144. G. J. McCarthy, *Acta Cryst.* 1971, **B27**,2285.

145. I. G. Wood, *J. Phys. C: Solid State Phys.* 1984, **17**, L539.

146. B. Y. Gu , H. Z. Cummins , S. L. Qiu, M. Copic, *Ferroelectrics* 1983, **52**, 45.

147. L. X. Pang, D. Zhou, Z. M. Qi, W. G. Liu, Z. X. Yue, I. M. Reaney, *J. Mater. Chem. C* 2017, **5**, 2695.

148. P. V. Bijumon, S. Solomon, M. T. Sebastian, P. Mohanan, *J. Mater. Sci.: Mater. Electro.*2003, **14**, 5.

149. F. Bertaut, A. Durif, *C.R. Acad. Sci.*1954, **238**, 2173.

150. A. Ennaciri, D. Michel, Y. Perez, M.Jorba, J. Pannetier, *Mater. Res. Bull.* 1984, **19**, 793.

151. M. Hirano, H. Morikawa, M. Inagaki, M. Toyoda, *J. Am. Ceram. Soc.* 2002, **85**, 1915.

152. M. Hirano, H. Morikawa, *Chem. Mater.* 2003, **15**, 2561.

153. X. Cheng, Y. Ren, J. Shang, Y. Song, *J. Phys. Chem. C* 2017, **121**, 723.

154. A. Ennaciri, A. Kahn, D. Michel, *J. Less-Common Metals*, 1986, **124**, 105.

155. A. Durif, *Acta Crystallogr.*1967, **1**,1948.

View Article Online
DOI: 10.1039/C8TC02260G

156. L. H. Brixner, A. W. Sleight, M. S. Licis. *J. Solid State Chem.*1972,**5**, 247.

157. T. Schustereit, T. Schleid, I. Hartenbach, *Acta Crystallogr. Sec. E.* 2013, **69**, pi7.

158. D. H. Templeton, A. Zalkin, *Acta Crystallogr.*1963, **16**, 762.

159. M. Cesari, G. Perego, A. Zazzetta, G. Manara, B. Notari. *J. Inorg. Nucl. Chem.*1971, **33**, 3595.

160. W. Jeitschko, *Acta Crystallogr.*1973, **B29**, 2074.

161. A. W. Sleight, W. J. Linn, *Ann. New York Academy Sci.* 1976, **272**, 22.

162. P. Porta, N. Franceschini, G. Minelli, *Mater. Chem. Phys.*2001, **70**, 17.

163. D. Zhou, W. B. Li, L. X. Pang, J. Guo, Z. M. Qi, T. Shao, X. Yao, C. A. Randall, *Dalton Trans.* 2014, **43**, 7290.

164. L. X. Pang, D. Zhou, W. G. Liu, Z. M. Qi, Z. X. Yue, *J. Eur. Ceram. Soc.*2018, **38**, 1535.

165. Z. Wang, C. Yuan, Q. Li, Q. Feng, F. Liu, Y. Yang, C. Zhou, G. Chen, *J. Electroceram.* 2017, https://doi.org/10.1007/s10832-017-0107-9.

166. K. Fukuda, R. Kitoh, I. Awai, *Jpn. J. Appl. Phys.*1993, **32**, 4584.

167. V. Subramanian, V. R. K. Murthy, B. Viswanathna, *Jpn. J.Appl. Phys.* 1997, **36**, 194.

168. P. L. Wise, I. M. Reaney, W. E. Lee, T. J. Price, D. M. Iddles, D. S. Cannell, *J. Eur. Ceram. Soc.* 2001, **21**, 1723.

169. H. L. Chen, C. L. Huang, *Jpn J. Appl. Phys.* 2002, **41**, 5650.

170. A. K Axelsson, M. T. Sebastian, M. N. Alford, *J. Korean Ceram. Soc.* 2003, **40**, 340.

171. K. H. Yoon, Y. H. Chang, W. S. Kim, J. B. Kim, E. S. Kim, *Jpn J. Appl. Phys.*1996, **35**, 5145.

View Article Online
DOI: 10.1039/C8TC02260G

172. D. Zhou, X. Q. Fan, X. W. Jin, D. W. He, G. H. Chen, *Inor. Chem.* 2016, **55**, 11979.

173. D. W. Kim, H. J. Youn, K. S. Hong, C.K. Kim, *Jpn. J. Appl. Phys.* 2002, **41**, 3812.

174. M. Touboul, C. Vachon, *Thermochim. Acta* 1988, **133**, 61.

175. P. W. Lv, M. Zheng, X. Wang, F. Huang, *J. Alloys Compd.* 2014, **583**, 285.

176. D. Zhou, D. Guo, W. B. Li, L. X. Pang, X. Yao, D. W. Wang, I. M. Reaney, *J. Mater. Chem. C* 2016, **4**, 5357.

177. L. X. Pang, H. Wang, D. Zhou, X. Yao, *J. Electroceram.* 2009, **23**, 13.

178. K. Fukuda, R. Kitoh, I. Awai, *Jpn. J. Appl. Phys.*1993, **32**, 4584.

179. L. Wu, Y. C. Chen, L. J. Chen, Y. P. Chou, Y. T. Tsai, *Jpn J. Appl. Phys.* 1999, **38**, 5612.

180. M. Valant, A. K. Axelsson, N. Alford, *J. Eur. Ceram. Soc.* 2007, **27**, 2549.

181. J. Guo, H. Guo, A. L. Baker, M. T. Lanagan, E. R. Kupp, G. L. Messing, C. A. Randall, *Angew. Chem., Int. Ed.* 2016, **55**, 11457.

182. D. W. Wang, D. Zhou, S. Y. Zhang, Y. Vardaxoglou, W. G. Whittow, D. Cadman, I. M. Reaney, *ACS Sustainable Chem. Eng.* 2018, **6**, 2438.

View Article Online
DOI: 10.1039/C8TC02260G

Table Captions:

Table 1 Sintering temperatures and microwave dielectric properties of the $(A^{+}_{0.5}A^{3+}_{0.5})BO_4$ (A^{+} = Li, Na, K and Ag; A^{3+} = Ln and Bi; B = Mo and W) ceramics

Table 2 Microwave dielectric ceramics with large permittivity and *TCF* (both negative and positive) values

View Article Online
DOI: 10.1039/C8TC02260G

Table 1 Sintering temperatures and microwave dielectric properties of the $(A^{+}_{0.5}A^{3+}_{0.5})BO_4$ (A^+ = Li, Na, K and Ag; A^{3+} = Ln and Bi; B = Mo and W) ceramics

Composition	R_A(Å)	R_B(Å)	S.T. (^oC)	ε_r	Q×f (GHz)	TCF (ppm/^oC)	Ref.
$(Li_{0.5}Yb_{0.5})MoO_4$	0.9525	0.41	820	16.3	6,350	+53	111
$(Li_{0.5}Er_{0.5})MoO_4$	0.962	0.41	800	18.6	10,650	+186	111
$(Li_{0.5}Y_{0.5})MoO_4$	0.9695	0.41	780	18.8	10,400	+193	111
$(Li_{0.5}Gd_{0.5})MoO_4$	0.9865	0.41	750	19.5	3,940	+209	111
$(Li_{0.5}Sm_{0.5})MoO_4$	0.9995	0.41	640	19.9	4,570	+231	111
$(Li_{0.5}Nd_{0.5})MoO_4$	1.0145	0.41	660	20.3	3,000	+235	111
$(Li_{0.5}Ce_{0.5})MoO_4$	1.0315	0.41	580	20.6	1,990	+228	111
$(Li_{0.5}Bi_{0.5})MoO_4$	1.045	0.41	560	41.7	3,200	+240	112
$(Na_{0.5}Bi_{0.5})MoO_4$	1.175	0.41	590	34.4	12,300	+43	112
$(Na_{0.5}La_{0.5})MoO_4$	1.17	0.41	740	11	25,050	−59	113
$(Na_{0.5}Nd_{0.5})MoO_4$	1.1445	0.41	760	10.5	19,605	−49	115
$(Na_{0.5}Ce_{0.5})MoO_4$	1.1615	0.41	780	11.2	19,365	−44	115
$(Ag_{0.5}Bi_{0.5})MoO_4$	1.225	0.41	690	30.4	12,600	+57	112
**$(K_{0.5}Bi_{0.5})MoO_4$	1.225	0.41	690	30.4	12,600	+57	112
*$(Li_{0.5}Bi_{0.5})$ WO_4	1.045	0.42	740	27.2	17,000	−56	116
$(Na_{0.5}Bi_{0.5})$ WO_4	1.175	0.42	720	25.7	17,500	-18	117
*$(Ag_{0.5}Bi_{0.5})WO_4$	1.225	0.42	580	35.9	13,000	-69	118
*$(Li_{0.5}Y_{0.5})WO_4$	0.9695	0.42	900	14.8	9,550	+64	119
*$(Li_{0.5}Yb_{0.5})WO_4$	0.9525	0.42	900	19.7	8,720	+45	119
$(Li_{0.5}Sm_{0.5})WO_4$	0.9995	0.42	800	17	5,792	+87	120

View Article Online
DOI: 10.1039/C8TC02260G

$(Li_{0.5}Nd_{0.5})WO_4$	1.0145	0.42	775	16.1	4,210	+162	121
$(Na_{0.5}Bi_{0.5})(Mo_{0.5}W_{0.5})O_4$	1.175	0.415	720	28.9	14,000	-6	117
$(Ag_{0.5}Bi_{0.5})(Mo_{0.5}W_{0.5})O_4$	1.225	0.415	580	26.3	10,000	+20	122

* marked crystallizes in wolframite structure; **$(K_{0.5}Bi_{0.5})MoO_4$ crystallizes in A site ordered structure.

View Article Online
DOI: 10.1039/C8TC02260G

Table 2 Microwave dielectric ceramics with large permittivity and *TCF* (both negative and positive) values

Compositions	S. T. (^{o}C)	Permittivity	*Qf* (GHz)	*TCF* (ppm/^{o}C)	Ref.
$BiVO_4$	820	68	8,000	–260	28,29
$Bi_2Ti_4O_{11}$	1100	47	4,800	–540	170
$(Li_{1/2}Ln_{1/2})TiO_3$	1300	80	3,100	–310	171
β-$BiTaO_4$	1300	53	12,070	–200	172
$BaNb_2O_6$ (Hex)	1050	42	4,000	–800	173
TiO_2	1350	100	>20,000	+400	166
$CaTiO_3$	1350	168	>10,000	+800	167-169
$SrTiO_3$	1350	280	3,000	+1200	167-169
$(Sr,Ba)TiO_3$	1350	>300	<2,000	>1200	179
*$Ag(Nb,Ta)O_3$	1250	>300	<800	——	180

*Due to the phase transition, TCF varies through large +/− values.

View Article Online
DOI: 10.1039/C8TC02260G

Figure Captions:

Fig. 1 a) Schematic of crystal structures of the orthorhombic[33,34]

Fig. 2 a) Crystal structure of tetragonal zircon phase of $BiVO_4$[33-36]

Fig. 3 Crystal structure of monoclinic scheelite phase of $BiVO_4$[33,34]

Fig. 4 Crystal structure of tetragonal scheelite phase of $BiVO_4$.[33,34]

Fig. 5 Phase transition diagram of the four polymorphs of $BiVO_4$[2-4,33,34,39-42,46,51-54]

Fig. 6 SEM micrographs of bismuth vanadates after firing with 20 wt. % of silver for 5 h at 750 ^oC: a) $BiVO_4$; b) $Bi_4V_2O_{11}$ and c) $Bi_8V_2O_{17}$) and 850 ^oC: d) $Bi_{12}V_2O_{23}$ and e) $Bi_{12}V_{0.6}O_{19.5}$).[28]

Fig. 7 X-ray diffraction patterns of Nd-doped $BiVO_4$ samples with the nominal stoichiometry $Nd_yBi_{1-y}VO_4$ ceramics[73]

Fig. 8 a) X-ray diffraction data for $(Bi_{1-x}Ce_x)VO_4$ (x = 0.1, 0.2, 0.25, 0.3, 0.4 and 0.6) ceramics and b) pseudo phase diagram of the $BiVO_4$-$CeVO_4$ system (* = scheelite monoclinic phase; and▼ = zircon type tetragonal phase)[74]

Fig. 9 Thermal expansion data of the $(Bi_{0.9}Ce_{0.1})VO_4$ ceramic* (*:unpublished data)

Fig. 10 X-ray diffraction patterns of $(Bi_{1-x}Dy_x)VO_4$ and $Bi_{0.5}M_{0.5}VO_4$ (M = La, Sm, Nd, Gd, Eu, Y)[78]

Fig. 11 a) XRD patterns of $(Bi_{1-x}Y_x)VO_4$ ceramics and b) phase diagram of the $BiVO_4$-YVO_4 binary system (Cell parameters a and b of $BiVO_4$ are 5.1 Å and 5.2 Å, respectively while cell parameters a/b of zircon phase is about a = b = 7.13 Å)[79,80]

Fig. 12 a) ε_r, *Qf*, *TCF* and sintering temperature of the $(Bi_{1-x}Y_x)VO_4$ ceramics as a function of x and b) range of ε_r obtained from infrared fitting[79,80]

Fig. 13 Schematic of phase composition diagram (room temperature) for the $(Bi_{1-x}A_x)VO_4$ system as a function of A ionic radius[61-83]

View Article Online
DOI: 10.1039/C8TC02260G

Fig. 14 XRD patterns of $BiVO_4$, In_2O_3 and $In_2O_3/BiVO_4$ composites with different molar ratios[86]

Fig. 15 Thermal expansion curves of the $(Bi_{1-x}Fe_x)VO_4$ (x = 0.06, 0.08, 0.10 and 0.20) ceramics as a function of temperature[87]

Fig. 16 Cell parameters and phase compositions of the $xBi(Fe_{1/3}Mo_{2/3})O_4$-$(1-x)BiVO_4$ system[56]

Fig. 17 Thermal expansion data of the $xBi(Fe_{1/3}Mo_{2/3})O_4$-$(1-x)BiVO_4$ (x = 0.0, 0.01, 0.02, and 0.04) as a function of temperature[56]

Fig. 18 Ferroelastic phase transition (monoclinic to tetragonal structure) temperature of the $xBi(Fe_{1/3}Mo_{2/3})O_4$-$(1-x)BiVO_4$ ceramics ($0.0 \leq x \leq 0.10$) as a function of x and for pure $BiVO_4$ as a function of pressure[46,56]

Fig. 19 Room temperature microwave dielectric properties of the $xBi(Fe_{1/3}Mo_{2/3})O_4$-$(1-x)BiVO_4$ ceramics ($0 \leq x \leq 1$)[56]

Fig. 20 Cell parameters and volume of $BiVO_4$ as a function of temperature and pressure and of $(1-x)BiVO_4$-$x(Li_{0.5}Bi_{0.5})MoO_4$ ceramics as a function of x at room temperature[32,46,124]

Fig. 21 a) ε_r and b) *Qf* of $(1-x)BiVO_4$-$x(Li_{0.5}Bi_{0.5})MoO_4$ ceramics from 10–420 K).[124]

Fig. 22 a) *In-situ* XRD, b) cell parameters and c) Raman spectra of $(1-x)BiVO_4$–$x(Li_{0.5}Bi_{0.5})MoO_4$ (x = 0.06) from 27–160 ^oC[126]

Fig. 23 a) Room temperature infrared spectra of $(1-x)BiVO_4$–$x(Li_{0.5}Bi_{0.5})MoO_4$ ($0.0 \leq x \leq 1.0$) ceramics, b) *in situ* infrared spectra of x = 0.06 and c) x = 0.125 from −183 to + 180 ^oC.[126]

Fig. 24 Cell parameters, *a* and *b*, of tetragonal phases in $(1-x)BiVO_4$-$x(K_{0.5}Bi_{0.5})MoO_4$ ceramics as a function of *x*.[57]

Fig. 25 XRD patterns of the $(1-x)BiVO_4$-$x(Li_{0.5}La_{0.5})MoO_4$ ceramics ($0 \leq x \leq 0.5$)

View Article Online
DOI: 10.1039/C8TC02260G

calcined at a) 800 ^{o}C and b) 0.8$BiVO_4$-0.2($Li_{0.5}Ln_{0.5}$)MoO_4 (Ln = La, Pr, Sm, Gd, Tb, Dy, Y, Yb and Lu) ceramics sintered at 850 ^{o}C.[130,131]

Fig. 26 Schematic room temperature phase composition diagram of the $BiVO_4$-$AMoO_4$ systems as a function of A site ionic radius.

Fig. 27 a) XRD patterns of the (1-x)$BiVO_4$-x$LaNbO_4$ ceramic sintered at different temperatures and b) schematic of the ABO_4 scheelite structure (release of distorted tetrahedra in the inset)[147]

Fig. 28 XRD patterns of the (1-x)$BiVO_4$-x$LaNbO_4$ ceramics sintered at different temperatures[147]

Fig. 29 Schematic of phase transitions between the zircon, scheelite, fergusonite, and monoclinic phases of $ZrGeO_4$ materials.[153]

Fig. 30 a) Ideal AMO_4 scheelite structure compared to three different A site ordered $A_{2/3}MoO_4$ structures: b) $La_{2/3}MoO_4$, c) $Eu_{2/3}MoO_4$ and d) $Bi_{2/3}MoO_4$ (Projections are half unit cells along the c axis of the ideal scheelite structure) [161]

Fig. 31 a) X-ray diffraction patterns for x$Bi_{2/3}MoO_4$–(1−x)$BiVO_4$ ($0.0 \leq x \leq 1.0$) ceramics sintered at different temperatures. In b) the merging of (101) and (011), (200) and (020) is marked by dashed lines) and the super-lattice diffraction peaks were marked. c) shows the ○: tetragonal scheelite phase, *: $Bi_{2/3}MoO_4$ monoclinic phases. d) reveals the cell parameters of scheelite phase as a function of x value (the four regions were distinguished by the cell parameters) and e) is a schematic structure of $BiVO_4$ (top) and $Bi_{2/3}MoO_4$ (bottom) with only half the unit cell shown in the ab-plane.[163]

Fig. 32 a) X-ray diffraction patterns of (1-x)$BiVO_4$-x$La_{2/3}MoO_4$ ($0.0 \leq x \leq 1.0$) ceramics calcined at different temperatures and b) cell parameters as a function of x value.[164]

Fig. 33 a) Schematic of phase diagram of the Bi_2O_3–TiO_2–V_2O_5 binary system after

View Article Online
DOI: 10.1039/C8TC02260G

Touboul and Lv's reports[174,175] and b) a promising region for temperature stable microwave dielectrics[176]

Fig. 34 Back-scattered electron images of the a) as-fired and b) fractured surfaces of the $0.45BiVO_4$-$0.55TiO_2$ ceramics sintered 2 h at 890 ^oC (The associated energy dispersive X-ray spectrum is inserted).[176]

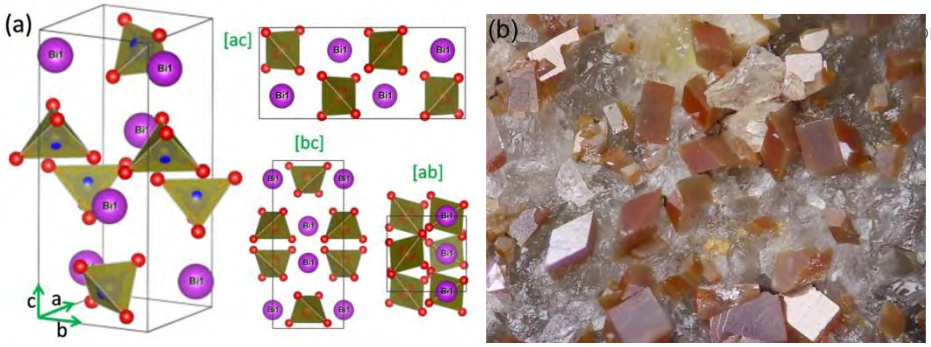

Fig. 1 a) Schematic of crystal structures of the orthorhombic and b) a image of the natural pucherite mineral[33,34]

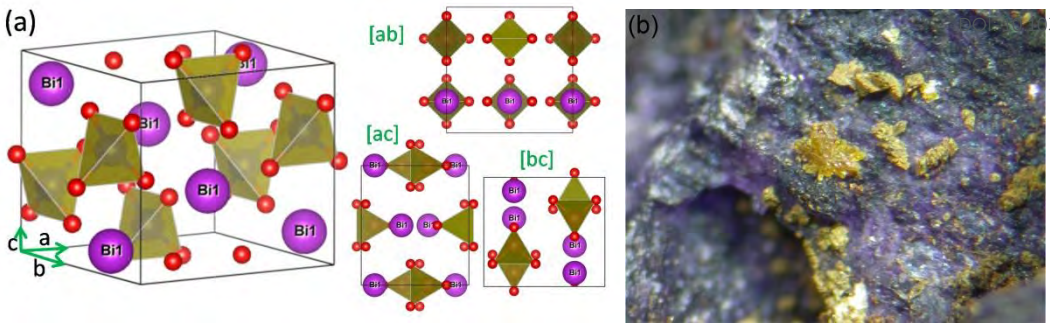

Fig. 2a) Crystal structure of tetragonal zircon phase of $BiVO_4$and b) an image of the mineral[33-36]

View Article Online
DOI: 10.1039/C8TC02260G

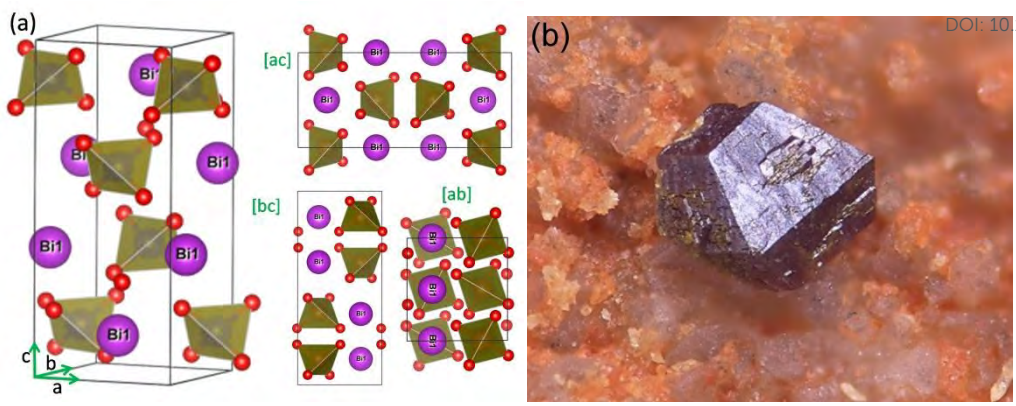

Fig. 3 Crystal structure of monoclinic scheelite phase of $BiVO_4$and b)an image of the mineral[33,34]

View Article Online
DOI: 10.1039/C8TC02260G

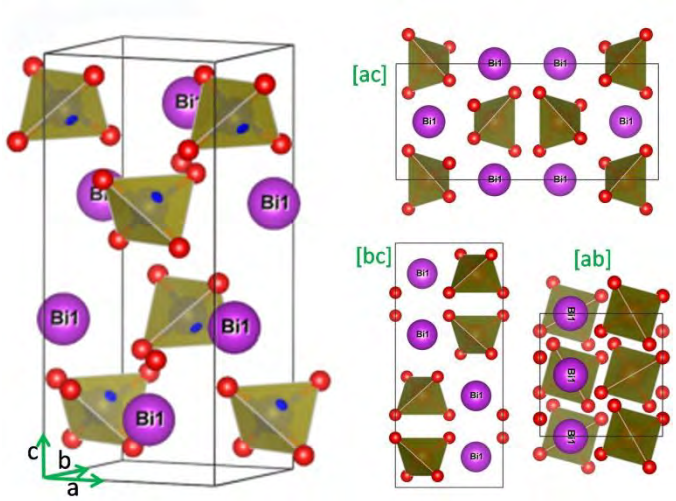

Fig. 4 Crystal structure of tetragonal scheelite phase of $BiVO_4$.[33,34]

View Article Online
DOI: 10.1039/C8TC02260G

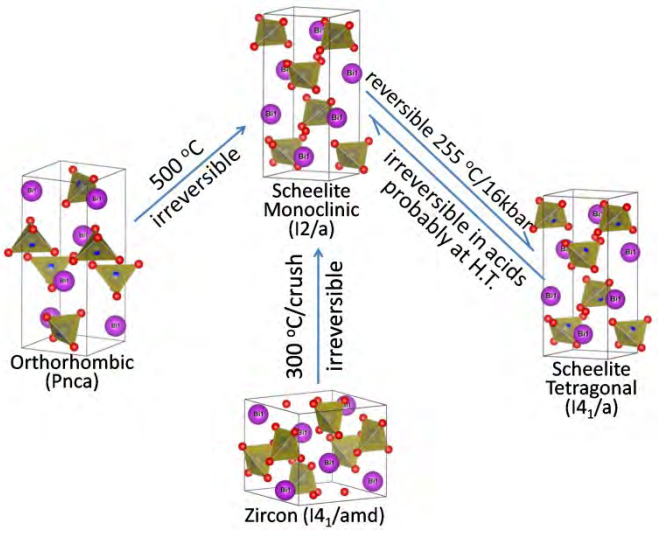

Fig. 5 Phase transition diagram of the four polymorphs of $BiVO_4$[2-4,33,34,39-42,46,51-54]

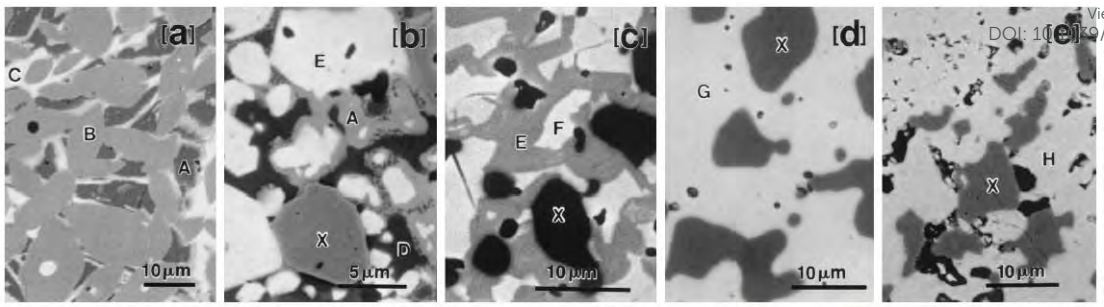

Fig. 6 SEM micrographs of bismuth vanadates after firing with 20 wt. % of silver for 5 h at 750 ^{o}C: a) $BiVO_4$; b) $Bi_4V_2O_{11}$ and c) $Bi_8V_2O_{17}$) and 850 ^{o}C: d) $Bi_{12}V_2O_{23}$ and e) $Bi_{12}V_{0.6}O_{19.5}$).[28]

View Article Online
DOI: 10.1039/C8TC02260G

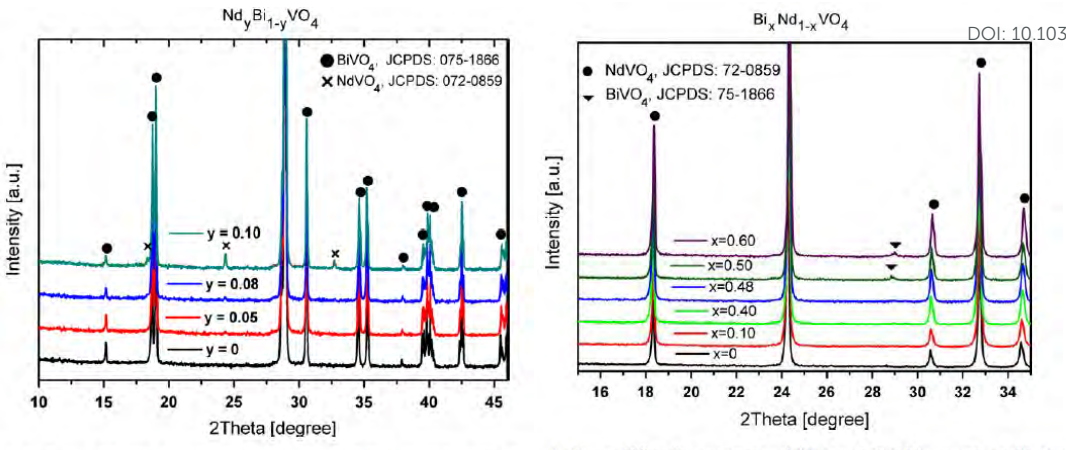

Fig. 7 X-ray diffraction patterns of Nd-doped $BiVO_4$ samples with the nominal stoichiometry $Nd_yBi_{1-y}VO_4$ ceramics[73]

View Article Online
DOI: 10.1039/C8TC02260G

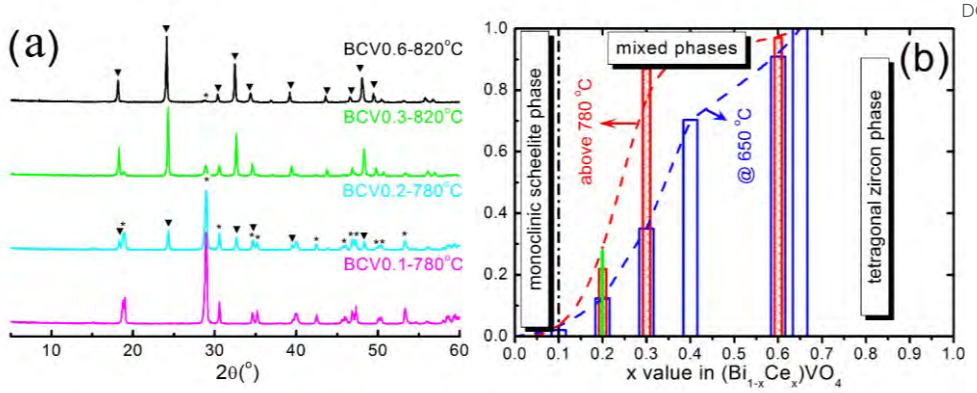

Fig. 8 a) X-ray diffraction data for $(Bi_{1-x}Ce_x)VO_4$ (x=0.1, 0.2, 0.25, 0.3, 0.4 and 0.6) ceramics and b) pseudo phase diagram of the $BiVO_4$-$CeVO_4$ system (* = scheelite monoclinic phase; and ▼ = zircon type tetragonal phase)[74]

View Article Online
DOI: 10.1039/C8TC02260G

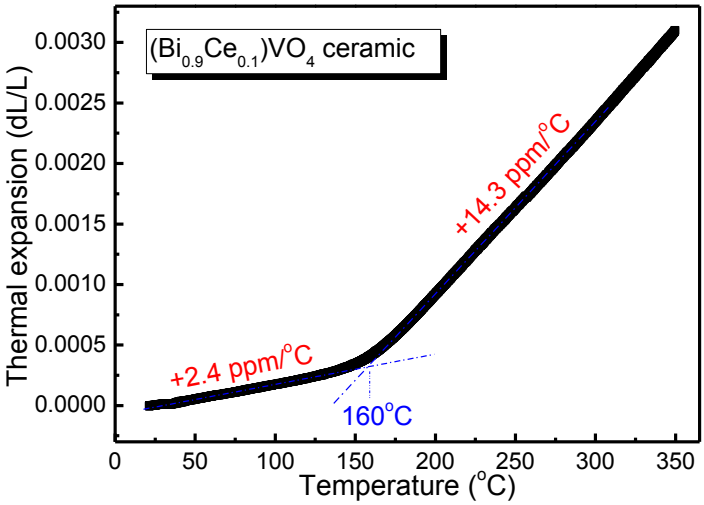

Fig. 9 Thermal expansion data of the $(Bi_{0.9}Ce_{0.1})VO_4$ ceramic* (*:unpublished data)

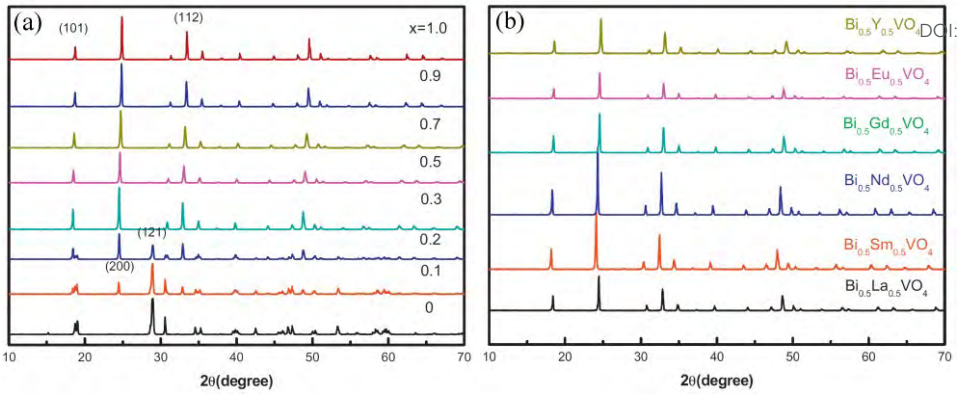

Fig. 10 X-ray diffraction patterns of $(Bi_{1-x}Dy_x)VO_4$and $Bi_{0.5}M_{0.5}VO_4$ (M=La, Sm, Nd, Gd, Eu, Y)[78]

View Article Online
DOI: 10.1039/C8TC02260G

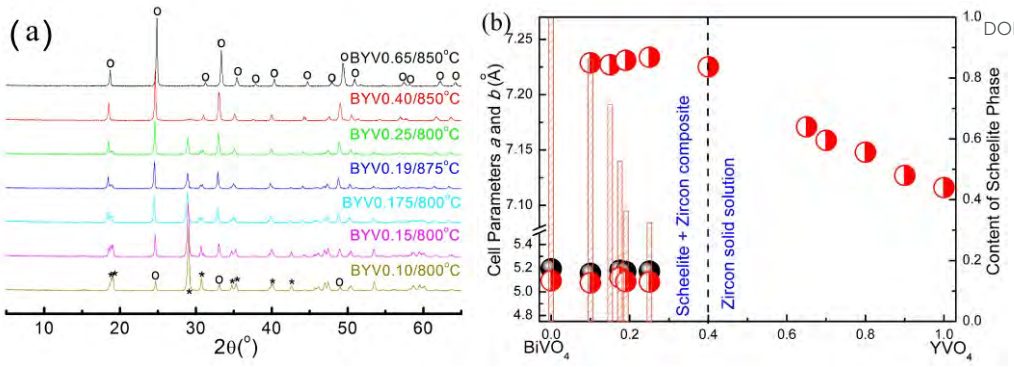

Fig. 11 a) XRD patterns of $(Bi_{1-x}Y_x)VO_4$ ceramics and b) phase diagram of the $BiVO_4$-YVO_4 binary system[79,80]

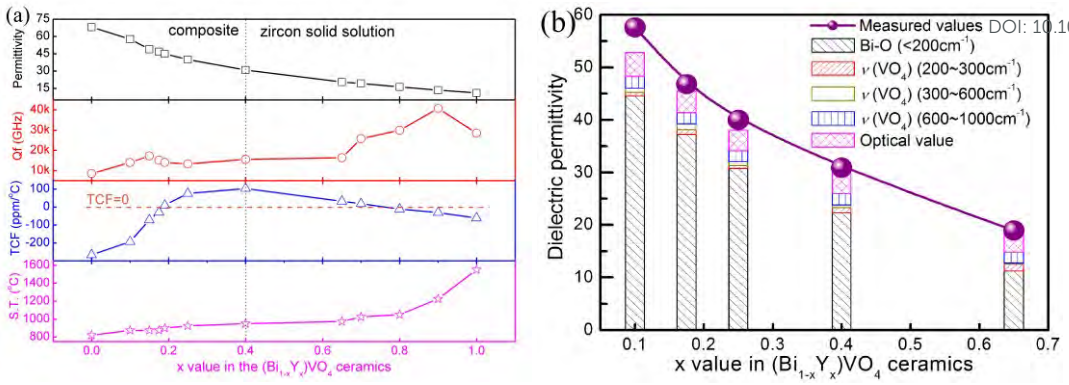

Fig. 12 a) ε_r, *Qf*, *TCF* and sintering temperature of the $(Bi_{1-x}Y_x)VO_4$ ceramics as a function of x and b) range of ε_r obtained from infrared fitting[79,80]

View Article Online
DOI: 10.1039/C8TC02260G

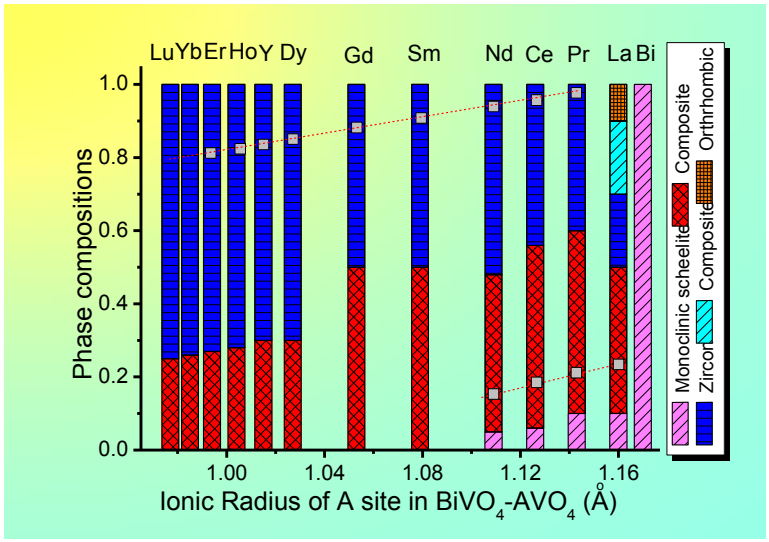

Fig. 13 Schematic of phase composition diagram (room temperature)for the $(Bi_{1-x}A_x)VO_4$ system as a function of A ionic radius.[61-83]

View Article Online
DOI: 10.1039/C8TC02260G

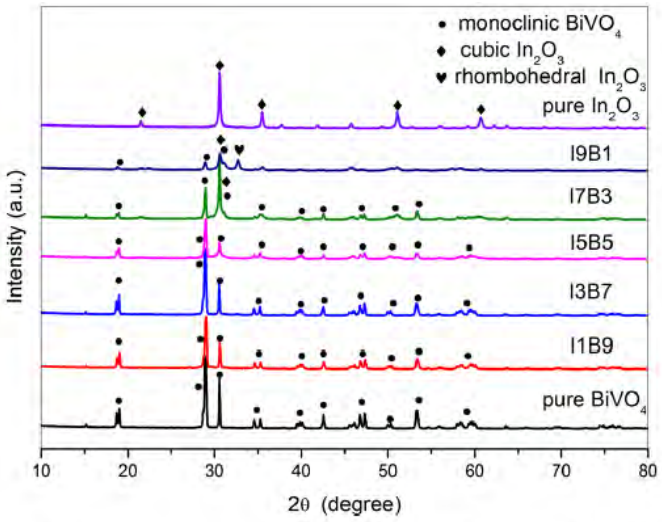

Fig. 14 XRD patterns of $BiVO_4$, In_2O_3 and $In_2O_3/BiVO_4$ composites with different molar ratios[86]

View Article Online
DOI: 10.1039/C8TC02260G

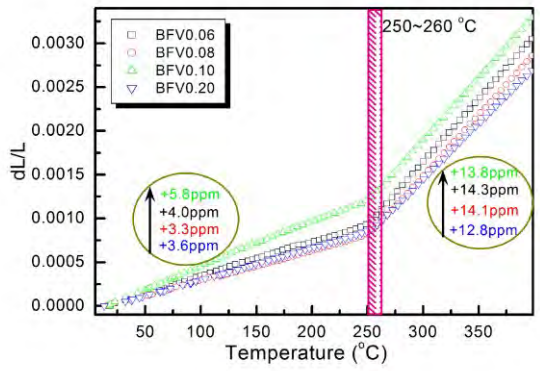

Fig. 15 Thermal expansion curves of the $(Bi_{1-x}Fe_x)VO_4$ (x=0.06, 0.08, 0.10 and 0.20) ceramics as a function of temperature[87]

View Article Online
DOI: 10.1039/C8TC02260G

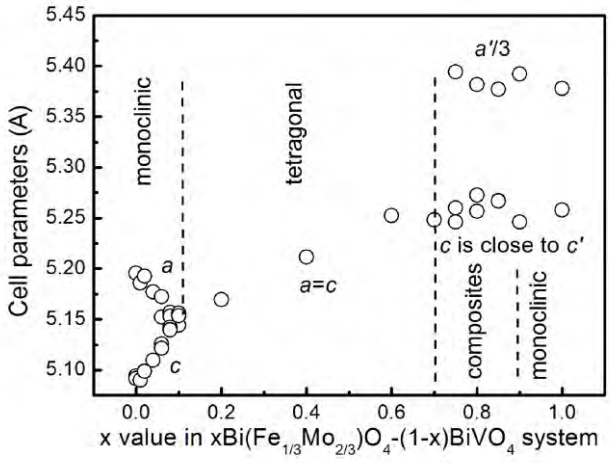

Fig. 16 Cell parameters and phase compositions of the $xBi(Fe_{1/3}Mo_{2/3})O_4$-$(1-x)BiVO_4$ system[56]

View Article Online
DOI: 10.1039/C8TC02260G

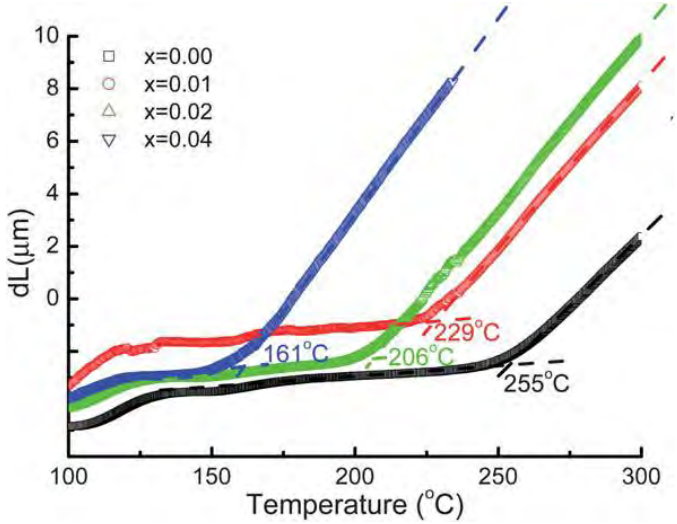

Fig. 17 Thermal expansion data of the $xBi(Fe_{1/3}Mo_{2/3})O_4$-(1-x)$BiVO_4$ (x=0.0, 0.01, 0.02, and 0.04) as a function of temperature[56]

View Article Online
DOI: 10.1039/C8TC02260G

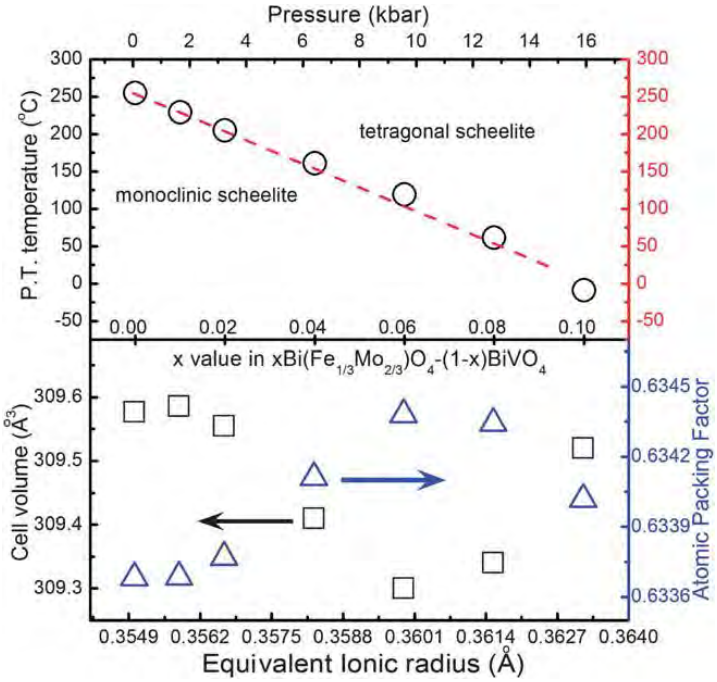

Fig. 18 Ferroelastic phase transition (monoclinic to tetragonal structure) temperature of the $xBi(Fe_{1/3}Mo_{2/3})O_4$-(1-x)$BiVO_4$ ceramics ($0.0 \leq x \leq 0.10$) as a function of x and for pure $BiVO_4$ as a function of pressure[46,56]

View Article Online
DOI: 10.1039/C8TC02260G

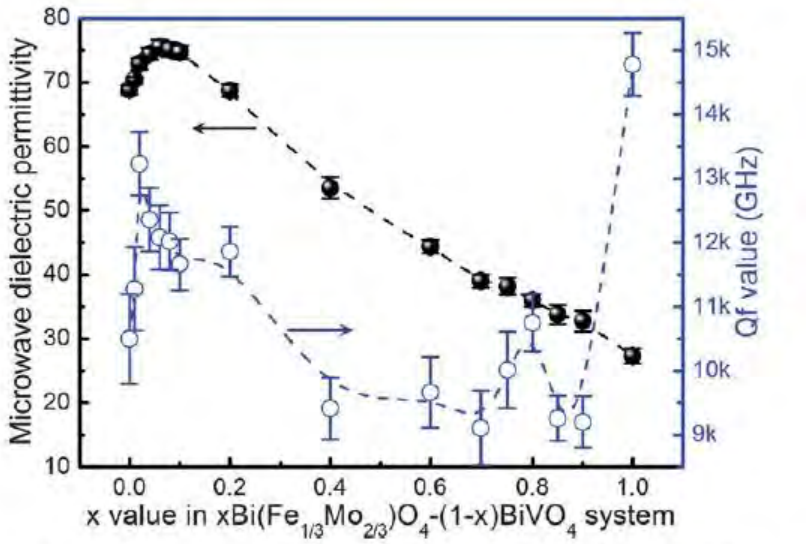

Fig. 19 Room temperature microwave dielectric properties of the $xBi(Fe_{1/3}Mo_{2/3})O_4$-$(1-x)BiVO_4$ ceramics ($0 \leq x \leq 1$)[56]

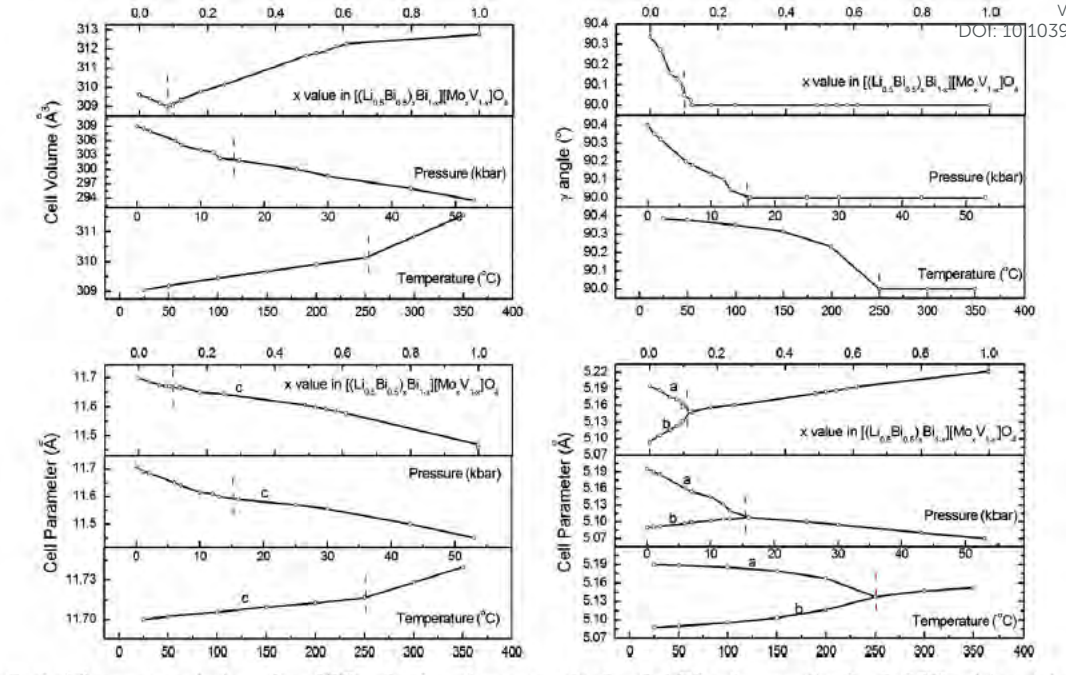

Fig. 20 Cell parameters and volume of $BiVO_4$ as a function of temperature and pressure and of$(1-x)BiVO_4$-$x(Li_{0.5}Bi_{0.5})MoO_4$ceramics as a function of x at room temperature[32,46,124]

View Article Online
DOI: 10.1039/C8TC02260G

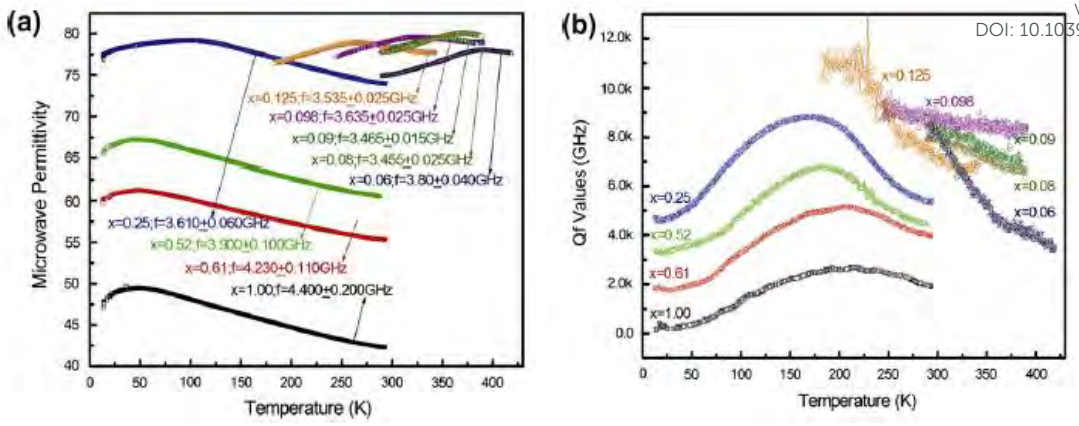

Fig. 21 a) ε_r and b) Qf of (1-x)$BiVO_4$-x($Li_{0.5}Bi_{0.5}$)MoO_4 ceramics from 10–420 K).[124]

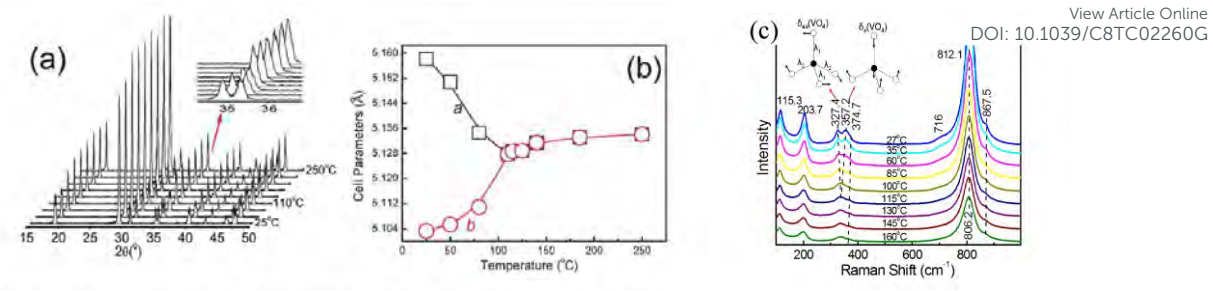

Fig. 22 a) *In-situ* XRD, b) cell parameters and c) Raman spectra of $(1\text{-}x)BiVO_4\text{–}x(Li_{0.5}Bi_{0.5})MoO_4$ (x = 0.06) from 27–160 ^oC[126]

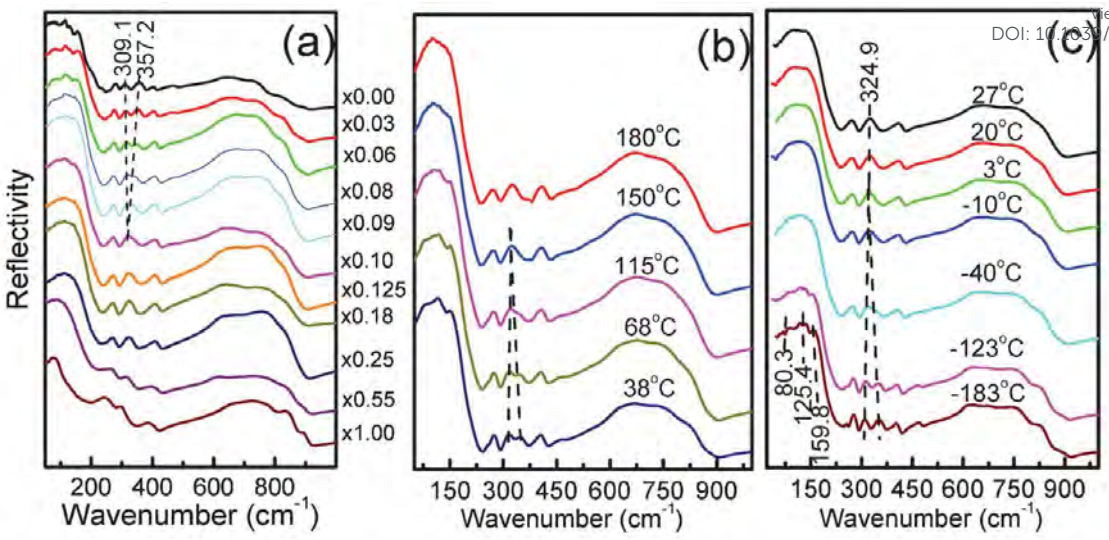

Fig. 23 a) Room temperature infrared spectra of (1-x)$BiVO_4$–x($Li_{0.5}Bi_{0.5}$)MoO_4 (0.0≤x ≤1.0) ceramics. b) in situ infrared spectra of x = 0.06 and c)x =0.125from −183 to +180 °C.[126]

View Article Online
DOI: 10.1039/C8TC02260G

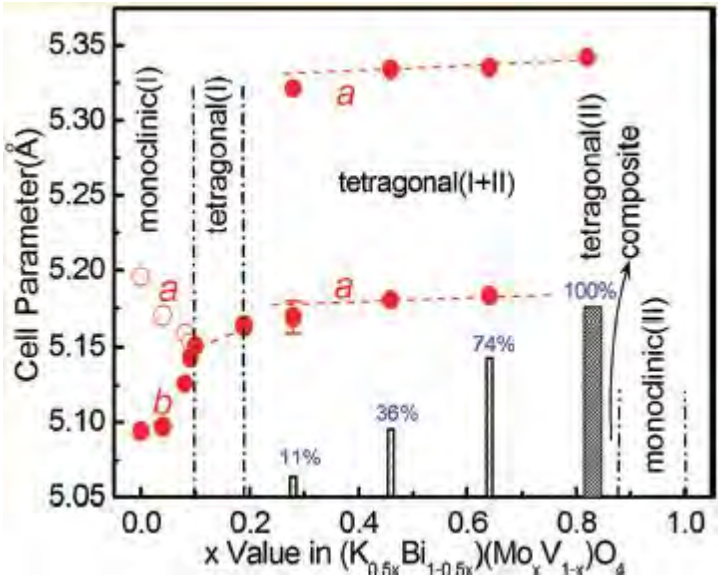

Fig. 24 Cell parameters, *a* and *b*, of tetragonal phases in (1-x)$BiVO_4$-x($K_{0.5}Bi_{0.5}$)MoO_4 ceramics as a function of *x*.[57]

View Article Online
DOI: 10.1039/C8TC02260G

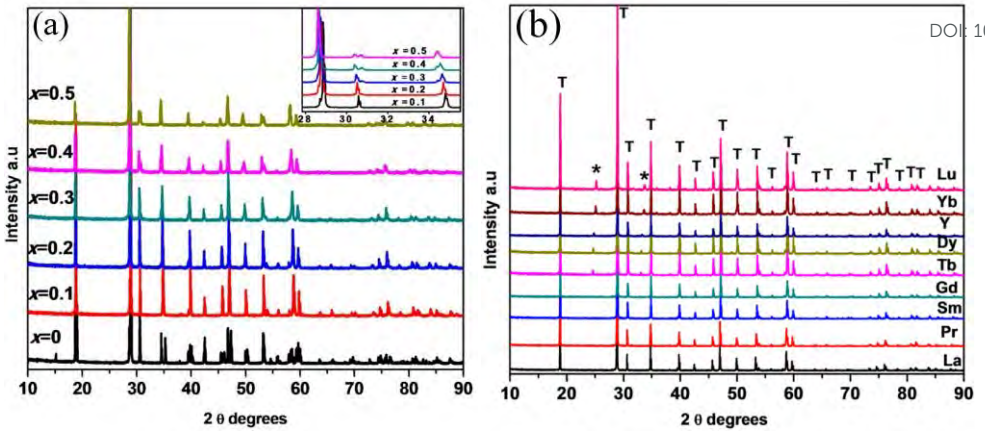

Fig. 25 XRD patterns of the (1-x)$BiVO_4$-x($Li_{0.5}La_{0.5}$)MoO_4 ceramics ($0 \leq x \leq 0.5$) calcined at a) 800 °C and b) 0.8$BiVO_4$-0.2($Li_{0.5}Ln_{0.5}$)MoO_4 (Ln=La, Pr, Sm, Gd, Tb, Dy, Y, Yb and Lu) ceramics sintered at 850 °C.[130,131]

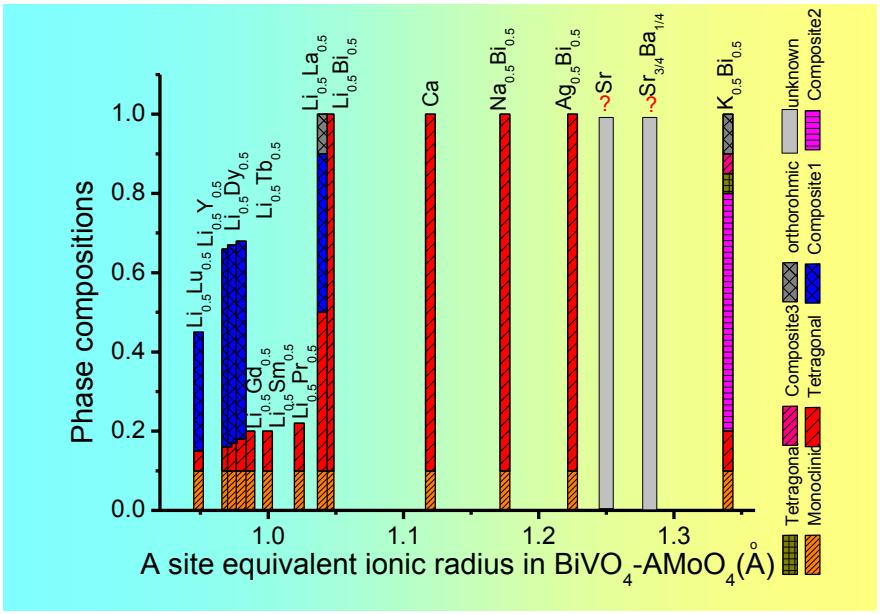

Fig. 26 Schematic room temperature phase composition diagram of the $BiVO_4$-$AMoO_4$ systems as a function of A site ionic radius.

View Article Online
DOI: 10.1039/C8TC02260G

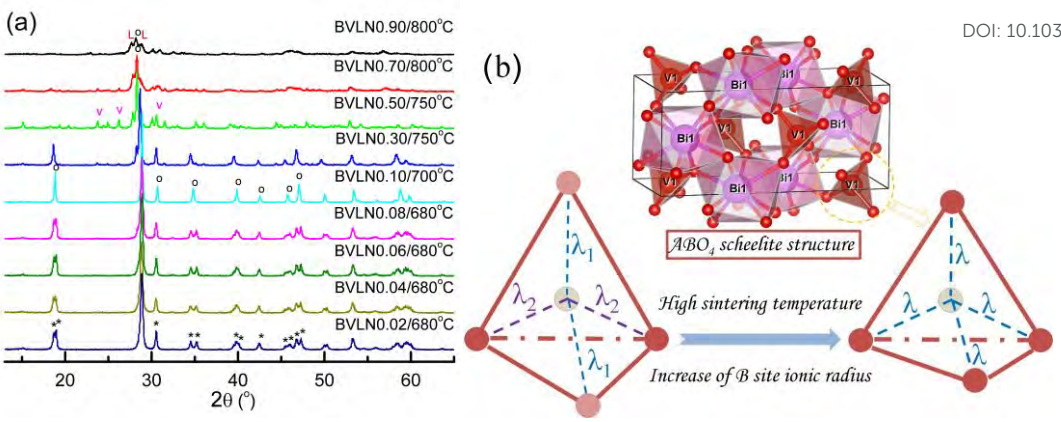

Fig. 27 a) XRD patterns of the (1-x)$BiVO_4$-x$LaNbO_4$ ceramic sintered at different temperatures and b) schematic of the ABO_4 scheelite structure (release of distorted tetrahedra in the inset)[147]

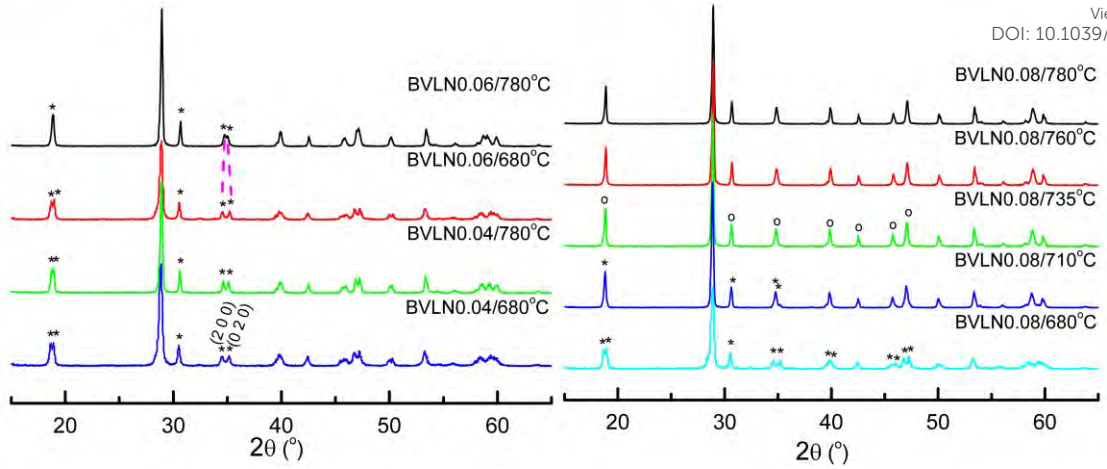

Fig. 28 XRD patterns of the (1-x)$BiVO_4$-x$LaNbO_4$ ceramics sintered at different temperatures[147]

View Article Online
DOI: 10.1039/C8TC02260G

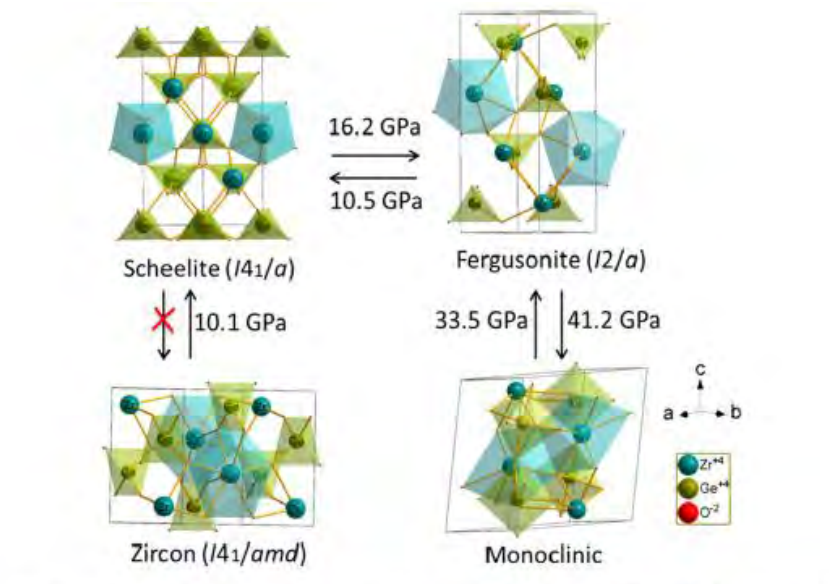

Fig. 29 Schematic of phase transitions between the zircon, scheelite, fergusonite, and monoclinic phases of $ZrGeO_4$ materials.[153]

View Article Online
DOI: 10.1039/C8TC02260G

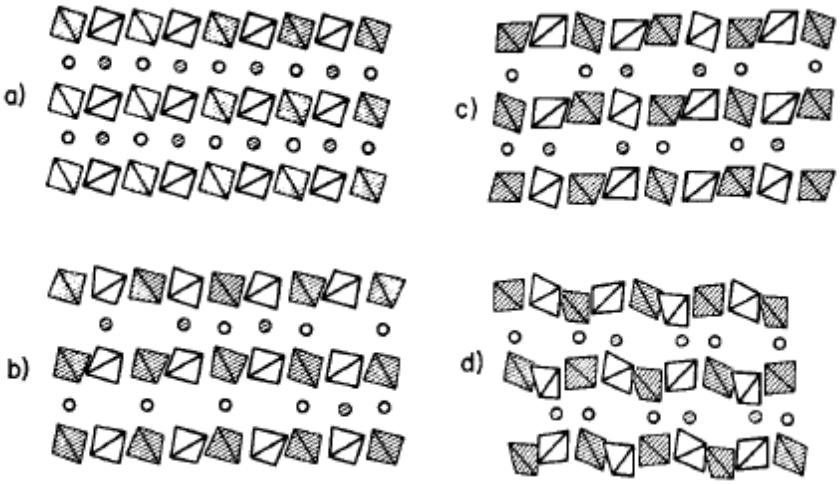

Fig. 30a) Ideal AMO_4 scheelite structure compared to three different A site ordered $A_{2/3}MoO_4$ structures: b) $La_{2/3}MoO_4$, c) $Eu_{2/3}MoO_4$ and d) $Bi_{2/3}MoO_4$(Projections are half unit cells along the c axis of the ideal scheelite structure) [161]

View Article Online
DOI: 10.1039/C8TC02260G

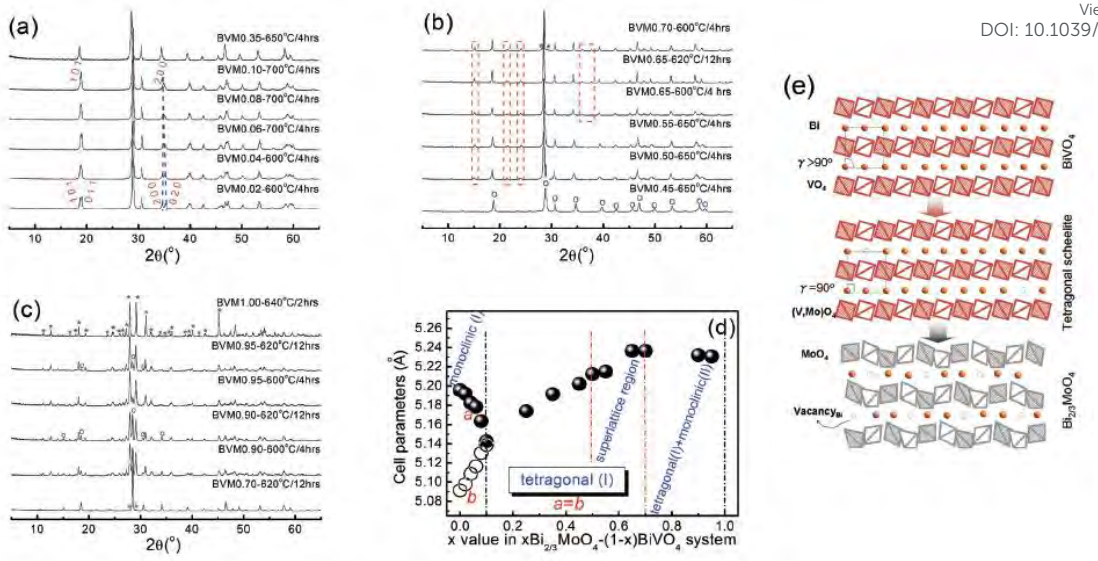

Fig. 31 a) X-ray diffraction patterns for $xBi_{2/3}MoO_4–(1−x)BiVO_4$ ($0.0 \leq x \leq 1.0$) ceramics sintered at different temperatures. In b) the merging of (101) and (011), (200) and (020) is marked by dashed lines) andthe super-lattice diffraction peaks were marked. c)shows the ○: tetragonal scheelite phase, *: $Bi_{2/3}MoO_4$ monoclinic phases. d) reveals the cell parameters of scheelite phase as a function of x value (the four regions were distinguished by the cell parameters) and e) is a schematic structure of $BiVO_4$ (top) and $Bi_{2/3}MoO_4$ (bottom) with only half the unit cell shown in the ab-plane.[163]

View Article Online
DOI: 10.1039/C8TC02260G

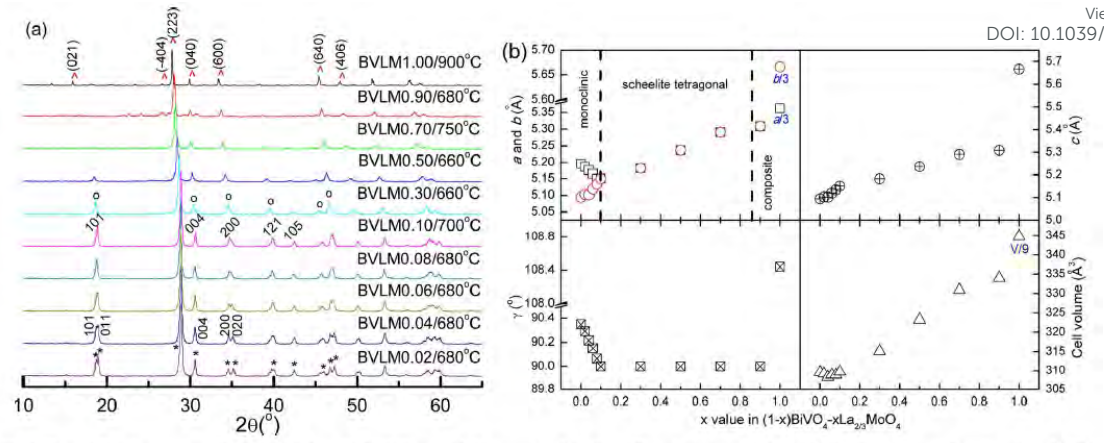

Fig 1. X-ray diffraction patterns of (1-x)$BiVO_4$-x$La_{2/3}MoO_4$ (0.0 ≤ x ≤ 1.0) ceramics calcined at different temperatures (a) and cell parameters as a function of x value (b).

Fig. 32 a) X-ray diffraction patterns of (1-x)BiVO4-x$La_{2/3}MoO_4$ (0.0 ≤x ≤1.0) ceramics calcined at different temperatures and b) cell parameters as a function of x value.[164]

View Article Online
DOI: 10.1039/C8TC02260G

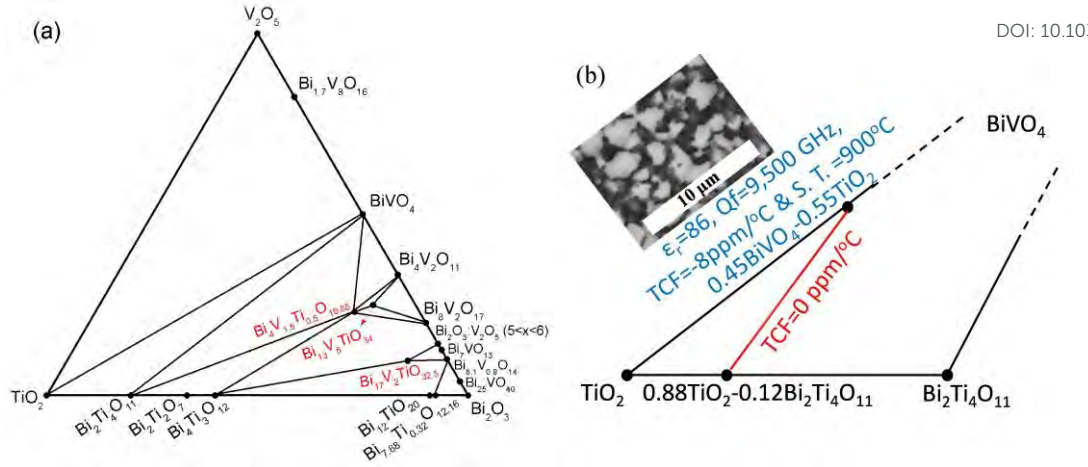

Fig. 33 a) Schematic of phase diagram of the Bi_2O_3–TiO_2–V_2O_5 binary system after Touboul and Lv's reports[174,175] and b) a promising region for temperature stable microwave dielectrics[176]

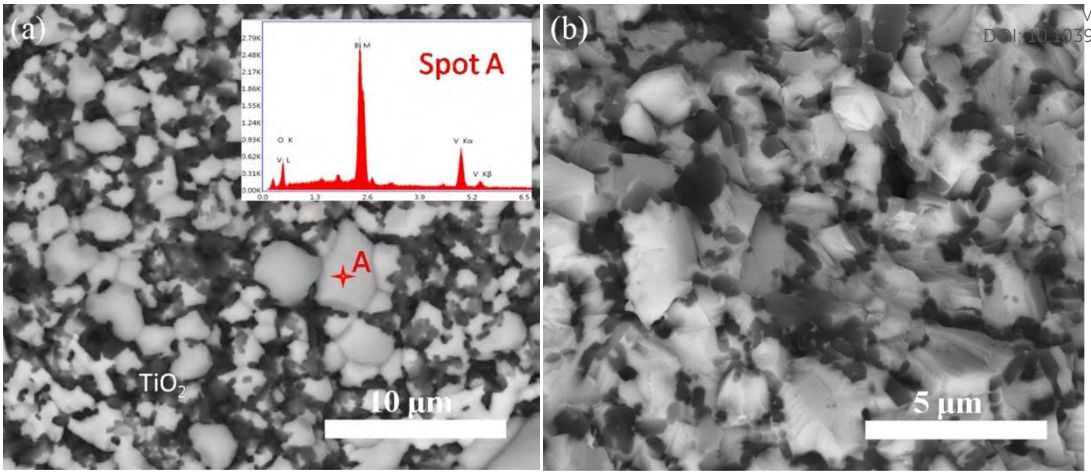

Fig. 34 Back-scattered electron images of the a) as-fired b) and fractured surfaces of the $0.45BiVO_4$-$0.55TiO_2$ ceramics sintered 2 h at 890 ^oC the associated energy dispersive X-ray spectrum is inserted).[176]

View Article Online
DOI: 10.1039/C8TC02260G

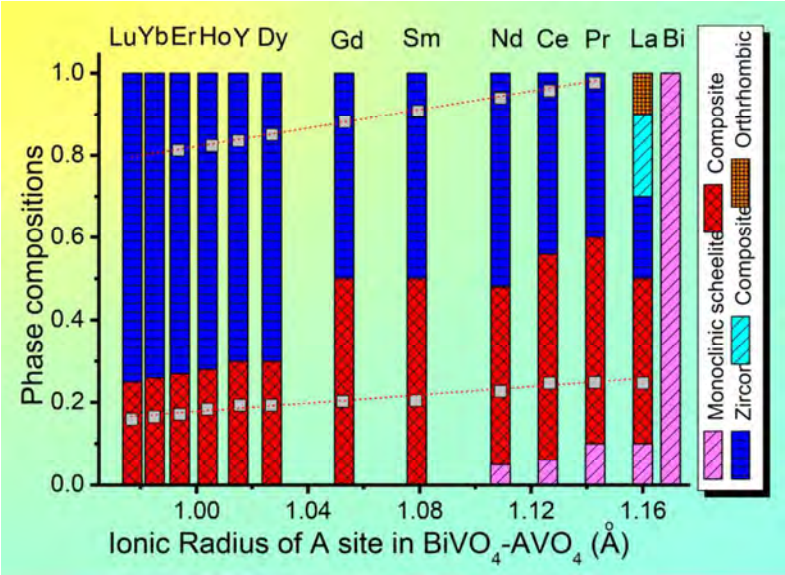

We precis recent studies on doped $BiVO_4$ ceramics in terms of A site, B site and A/B site complex substitutions. Low sintering temperature (< 800 ^oC), high ε_r and near temperature coefficient zero values could be obtained in solid solution and composite ceramics.